JEM Journal of Experimental Medicine

ARTICLE

Extensive dissemination and intraclonal maturation of HIV Env vaccine-induced B cell responses

Ganesh E. Phad[1], Pradeepa Pushparaj[1], Karen Tran[2], Viktoriya Dubrovskaya[2], Monika Àdori[1], Paola Martinez-Murillo[1], Néstor Vázquez Bernat[1], Suruchi Singh[3], Gilman Dionne[4], Sijy O'Dell[5], Komal Bhullar[1], Sanjana Narang[1], Chiara Sorini[6], Eduardo J. Villablanca[6], Christopher Sundling[6], Benjamin Murrell[1], John R. Mascola[5], Lawrence Shapiro[4], Marie Pancera[3], Marcel Martin[7], Martin Corcoran[1], Richard T. Wyatt[2], and Gunilla B. Karlsson Hedestam[1]

Well-ordered HIV-1 envelope glycoprotein (Env) trimers are prioritized for clinical evaluation, and there is a need for an improved understanding about how elicited B cell responses evolve following immunization. To accomplish this, we prime-boosted rhesus macaques with clade C NFL trimers and identified 180 unique Ab lineages from ∼1,000 single-sorted Env-specific memory B cells. We traced all lineages in high-throughput heavy chain (HC) repertoire (Rep-seq) data generated from multiple immune compartments and time points and expressed several as monoclonal Abs (mAbs). Our results revealed broad dissemination and high levels of somatic hypermutation (SHM) of most lineages, including tier 2 virus neutralizing lineages, following boosting. SHM was highest in the Ab complementarity determining regions (CDRs) but also surprisingly high in the framework regions (FRs), especially FR3. Our results demonstrate the capacity of the immune system to affinity-mature large numbers of Env-specific B cell lineages simultaneously, supporting the use of regimens consisting of repeated boosts to improve each Ab, even those belonging to less expanded lineages.

Introduction

Traditional assessments of vaccine-induced antibody (Ab) responses rely on serological assays to determine if immunization has induced the desired Ab specificity and potency. However, measurement of serum Igs does not reveal information about the specific Ab variable (V), diversity (D), and joining (J) segment gene rearrangements responsible for the antigen-specific response, nor about the underlying dynamics and maturation of the responding B cell populations. For a deeper understanding of vaccine-induced B cell responses, we developed protocols for antigen-specific single memory B cell sorting and mAb isolation from immunized rhesus macaques. These studies revealed the targeted epitopes and the mode of recognition by their cognate Abs, providing information that will help guide the design of improved immunogens and immunization protocols (Martinez-Murillo et al., 2017; Navis et al., 2014; Phad et al., 2015; Sundling et al., 2012a). However, the isolation of mAbs is low throughput and typically identifies only one or a few somatic variants from each Ab lineage, yielding limited information about the maturation of the response at the clonal level. In contrast, high-throughput Ab repertoire sequencing (Rep-seq) enables analyses of millions of B cells per sample, allowing definition of large numbers of clonally related sequences and more comprehensive understanding of Ab responses (Davydov et al., 2018; Galson et al., 2014; Georgiou et al., 2014; Jiang et al., 2013; Wiley et al., 2011; Yermanos et al., 2018). The use of Rep-seq is especially valuable if antigen-specific lineages can be identified in the data, as has been demonstrated for HIV-1 infection–induced Ab that undergo extensive affinity maturation (Bonsignori et al., 2016; Doria-Rose et al., 2014; Wu et al., 2015).

The examination of genetic properties of elicited Abs relies on the availability of comprehensive and validated reference databases of Ab VDJ germline gene segments. Even more than humans, rhesus macaques are highly diverse at both their MHC (Shen et al., 2013) and Ab VDJ loci (Corcoran et al., 2016). A comprehensive public reference database of macaque Ab germline genes is not yet available despite recent efforts (Cirelli et al., 2019; Corcoran et al., 2016; Francica et al., 2015; Ramesh et al., 2017). Definition of the specific VDJ alleles present in a

[1]Department of Microbiology, Tumor and Cell Biology, Karolinska Institutet, Stockholm, Sweden; [2]International AIDS Vaccine Initiative, Neutralizing Antibody Center, Department of Immunology and Microbiology, The Scripps Research Institute, La Jolla, CA; [3]Vaccine and Infectious Disease Division, Fred Hutchinson Cancer Research Center, Seattle, WA; [4]Department of Biochemistry and Molecular Biophysics, Columbia University, New York, NY; [5]Vaccine Research Center, National Institute of Allergy and Infectious Diseases, National Institutes of Health, Bethesda, MD; [6]Department of Medicine, Solna, Karolinska Institutet and Karolinska University Hospital, Stockholm, Sweden; [7]Science for Life Laboratory, Department of Biochemistry and Biophysics, Stockholm University, Stockholm, Sweden.

Correspondence to Gunilla B. Karlsson Hedestam: gunilla.karlsson.hedestam@ki.se.

given animal is necessary for correct Ab gene assignments, precise determination of somatic hypermutation (SHM), and definition of B cell clonal relationships (Yaari and Kleinstein, 2015), a prerequisite for B cell lineage-tracing studies. To meet this need, we developed IgDiscover, a computational tool allowing rapid generation of individualized Ab germline gene databases for both humans and rhesus macaques (Corcoran et al., 2016).

While the induction of cross-neutralizing HIV-1 Abs through immunization has proven extremely challenging (reviewed in Kwong et al., 2013), persistent efforts have resulted in the design of well-ordered soluble HIV-1 envelope glycoprotein (Env) trimers that closely mimic the native HIV-1 spike (Guenaga et al., 2017; Julien et al., 2013), infusing new optimism in the field. In initial studies, these trimers elicited strain-restricted neutralizing Abs against difficult-to-neutralize (tier 2) clinical HIV-1 isolates (Martinez-Murillo et al., 2017; Pauthner et al., 2017; Sanders et al., 2015), and recent work demonstrated that such responses protect against homologous chimeric simian-human immunodeficiency virus challenge (Pauthner et al., 2019). Several studies are now underway to evaluate the response elicited by a variety of well-ordered trimers, with or without epitope-focused immunogens as a prime (Kong et al., 2019; Xu et al., 2018), in small animal, macaque, or human clinical trials. A major objective of these studies is to induce Ab responses against conserved Env epitopes, such as those defined by broadly neutralizing Abs identified in HIV-1–infected individuals (Huang et al., 2012, 2014; Kong et al., 2016; Scheid et al., 2011; Walker et al., 2011; Wu et al., 2010).

To investigate the dynamics and evolution of the B cell response elicited by Env, we combined single B cell sequencing of Ab heavy chain (HC) sequences with high-throughput bulk repertoire sequencing and Ab lineage tracing analysis. We used the native-like flexibly linked (NFL) trimers derived from a clade C clinical isolate, 16055 (Guenaga et al., 2017), which we previously showed elicited autologous tier 2 neutralizing Ab responses that target the Env V2 region (Martinez-Murillo et al., 2017). We selected the animal that responded best to the vaccination, D20, for an in-depth investigation of the response, akin to Ab tracing studies performed in single HIV-1–infected patients, except that we traced a highly polyclonal response and not just one or a few Ab lineages. We generated Rep-seq data from multiple time points and immune compartments, and we used the IgDiscover software to define the specific germline alleles present in D20 to ensure correct gene assignments, clonal grouping, and SHM calculations.

Our analysis revealed broad dissemination of the response in the draining LN, spleen, blood, and bone marrow (BM), with increasing SHM levels following boosting for almost all lineages analyzed, independent of the expansion level of the lineage. Interestingly, the SHM was not restricted to the complementarity determining regions (CDRs), as numerous mutations also accumulated in the framework regions (FRs), especially in FR3. Functional analysis of variants belonging to a neutralizing Ab lineage targeting the V2 apex of the 16055 Env spike, the GM9_TH8 lineage, showed that enhanced neutralizing potency against the autologous virus was associated with increasing SHM, including residues located in the FR3. These data demonstrate the positive impact of the affinity maturation process on the evolving polyclonal Ab response following repeated boosting.

Results

Env-specific single memory B cell sorting and sequencing identified multiple Ab clonotypes

Previously, we demonstrated the capacity of the well-ordered 16055 NFL Env trimers (Guenaga et al., 2017) to elicit HIV-1 autologous tier 2 neutralizing Abs, which mapped to the V2 region of Env (Martinez-Murillo et al., 2017). Here, we inoculated four macaques (D15, D16, D19, and D20) with trimers in the Matrix-M adjuvant i.m. at weeks 0, 4, 12, 24, 36, and 45 (Fig. 1 A, left). We first administered 16055Δgly4 NFL Env trimers lacking sites for N-linked glycosylation proximal to the CD4 binding site (CD4bs; Dubrovskaya et al., 2017), and we then boosted with WT NFL Env trimers (16055wt) as described in Fig. 1 A. Blood samples were collected 2 wk after each inoculation for analysis of neutralizing Ab activity. All four animals developed plasma tier 2 16055 autologous neutralizing titers, with D20 displaying the most potent response (Fig. 1 A, right). We selected this animal for a comprehensive analysis of the Ab response and sorted Env-specific single memory B cells from peripheral blood mononuclear cells (PBMCs) from the last time point, 2 wk after the sixth immunization. We stained Env-specific memory B cells using a panel of Abs previously shown to cross-react with macaque memory B cells (Sundling et al., 2010) and a C-terminally biotinylated Env trimer probe identical to the 16055 NFL trimer immunogen, except for the presence of a C-terminal Avi-tag. Using FACS, we sorted ∼1,000 single Env-specific $CD20^+IgG^+CD27^+$ B cells (Fig. 1 B), from which we obtained 672 full-length HC VDJ sequences by Sanger sequencing. For a summary of the sorting statistics and FACS gating panels, see supplemental material (Fig. S1, A and B).

We next collected preimmunization blood samples and sequenced an IgM library from D20 to generate an individualized germline gene database using the IgDiscover software as previously described (Corcoran et al., 2016; Fig. S1 C). We assigned the 672 Env-specific HC sequences isolated from the time point after the sixth immunization (post-6) to the specific germline VH and JH alleles derived from D20 using the individualized database and calculated the level of SHM for each region (Fig. 1, C and D). This analysis demonstrated that the Env-specific B cells used a broad range of alleles, consistent with our previous studies using an earlier-generation Env trimer immunogen (Sundling et al., 2014). Several of the HC sequences were highly mutated, with SHM levels ranging from 5 to 15% at the nucleotide level (Fig. 1, C and D).

We next determined the number of unique B cell clonotypes present among the 672 Env-specific HC sequences. We defined Ab clonotypes as follows: identical V and J allele assignments, identical HCDR3 length, 80% HCDR3 amino acid homology, and at least one junction with no mismatches (called the "80%*" criterion). We included the junction matching requirement because the junctions are an important feature of clonal identity.

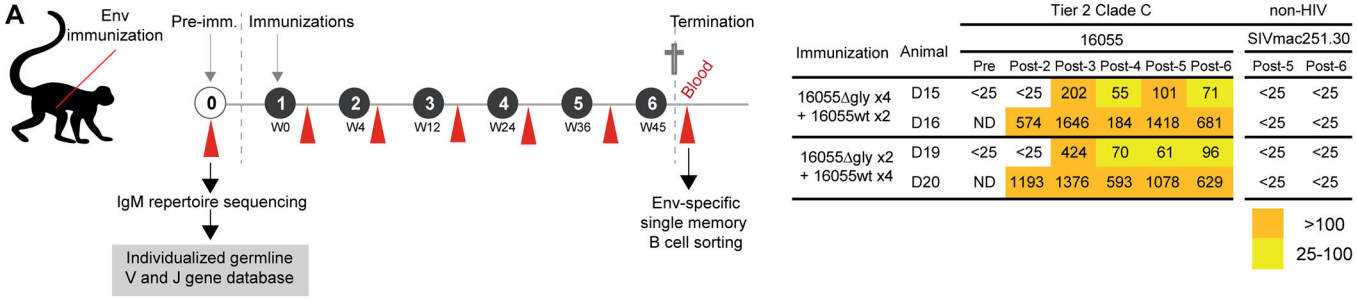

Immunization	Animal	Tier 2 Clade C 16055 Pre	Post-2	Post-3	Post-4	Post-5	Post-6	non-HIV SIVmac251.30 Post-5	Post-6
16055Δgly x4 + 16055wt x2	D15	<25	<25	202	55	101	71	<25	<25
	D16	ND	574	1646	184	1418	681	<25	<25
16055Δgly x2 + 16055wt x4	D19	<25	<25	424	70	61	96	<25	<25
	D20	ND	1193	1376	593	1078	629	<25	<25

>100
25-100

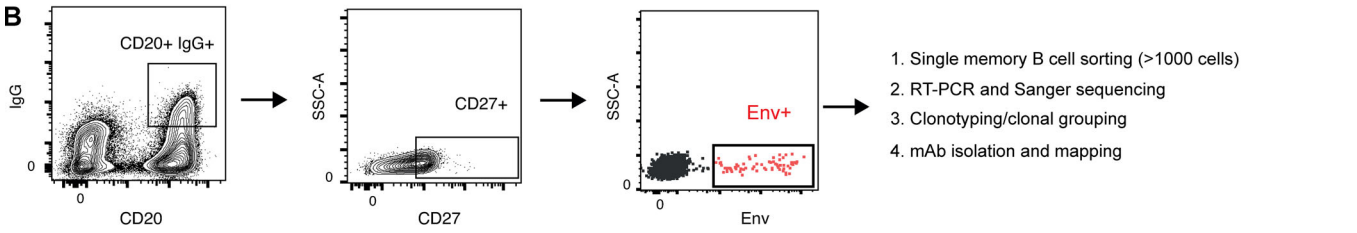

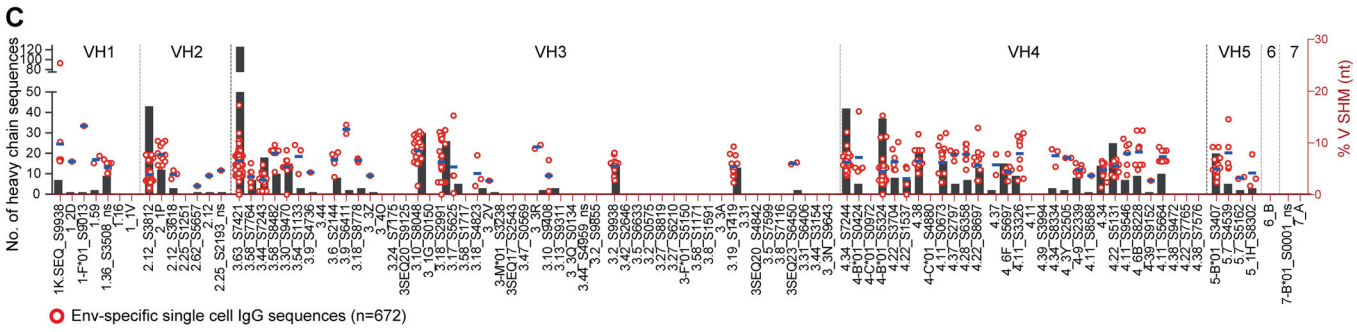

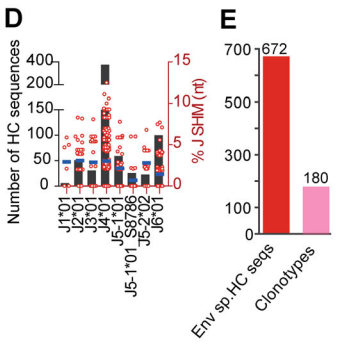

F

MAb ID	VH	JH	HCDR3	%VH SHM (nt)	VK/VL	JK/JL	LCDR3	%VK/VL SHM (nt)	Virus neutralization Tier 1 HxB2	DJ263	MW965	Tier 2 16055
GM9_TH8*	4.11_S5664	5-1*01_S8786	ARGLWSGYFFWFDV	6.5	lib4kappa_12	JK2*01	LQDYSTPYT	4.6	>50	>50	>50	0.012
GM3_TC2*	3.10_S8048	5-1*01	TTASYFNENGYISYNRFDV	12.2	VL6-2*02	JL6*01	QSTNDNSNPV	10	>50	>50	>50	0.102
GM6_TG1*	2_1P	4*01	SRGYGYDYAYLPFEY	10.4	lib7lambda_10	JL6*01	YFGDGHNHV	13.9	>50	>50	>50	1.05
GM7_TE9*	5-B*01_S3407	4*01	ARLEFSWDDVPAVGY	4.8	VL1-8*01	JL3*01	EVWESSLSGPL	7.8	>50	>50	0.005	>50
GM7_TH2*	4_6F_S5697	4*01	ARFSGLHSVAVFEY	5.4	VL3-2*01	JL3*01	NSWDSSGTHLL	3.1	>50	0.398	0.014	>50
GM11_TH2	2.12_S3618	5-1*01_S8786	ARAPVVGYCSGLVCYAGEWFDV	4.7	lib9kappa_32	JK1*01	LQSKNSPWT	4.7	>50	>50	>50	>50
GM1_TH1	3.44_S7243	3*01	ARGGRIYNPWTAKYSLGAIDF	4.4	lib4kappa_12	JK4*01	LQDYTPSLT	3.6	>50	>50	>50	>50
GM5_TD1	3.54_S1133	6*01	ARERPPSTVPVVFDLVYFGLDS	9.6	lib7lambda_14	JL2*01	QSYDSSLIGRV	4.8	>50	>50	>50	>50
GM4_TD7†	3.63_S7421	4*01	VKGGWGH	5.8	lib7lambda_14	JL2*01	LLYYSGSWV	4.1	>50	>50	>50	>50
GM9_TD2†	3.63_S7421	4*01	VKGGWGH	10.4	lib7lambda_14	JL2*01	LLYFSGAWV	4.8	>50	>50	>50	>50
GM4_TD9†	3.63_S7421	4*01	VKGGWGH	7.5	lib7lambda_14	JL2*01	LLYFSGAWV	4.8	>50	>50	>50	>50
GM2_TD2	3.63_S7421	2*01	AKEAYSGTYYRWYFDV	5.8	lib6kappa_17	JK4*01	QQYSNWPLT	3.2	>50	>50	>50	>50
GM9_TH5	4.38	2*01	VGSPDWTGNGPSKHWYFDL	8.6	VK2S12*01	JK4*01	QQETNWAVS	5.3	>50	>50	>50	>50
GM10_TD6	4_6F_S5697	4*01	ATLPGY	9.9	VK2S18*01	JKJ2*01	MQGRRSPYS	5.4	>50	>50	>50	>50
GM5_TF7	4.34_S7244	4*01	ARDVRPVAAIRDFDS	8	VL7-2*01	JL2*01	LLYYSGARV	4.1	>50	>50	>50	>50
GM11_TG8	4.34_S7244	2*01	ARTIGVTTRWSFGL	4	VL2-7*01	JL2*01	SSFAGSYTFF	2.4	>50	>50	>50	>50
GM5_TH10	5.7_S5162	6*01	AKGFSGYFRYGLDS	3.1	VK2S12*01	JK4*01	MQHKALPLT	2.3	>50	>50	>50	>50

*Neutralizing lineages †Clonal variants

IC50 μg/ml ≤0.015 .015-.100 .100-1.00

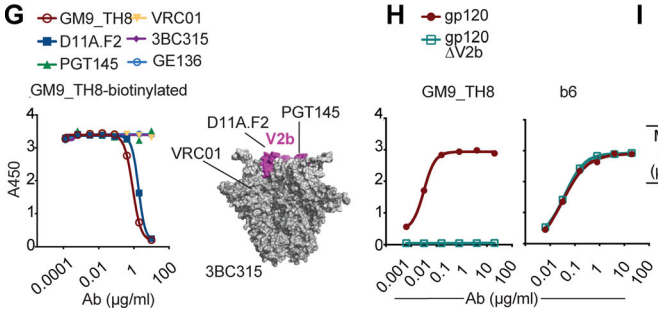

I

V2b:[180] DIVPLEEERKGNSSKYRLI[194]

V2b Ala mutatnts

		16055 WT	V182A	P183A	L184A	E185A	E186A	E186aA	R186bA	K186cA	G186dA
MAbs IC50 (μg/ml)	D11A.F2	4.43	10.64	>50	5.20	>50	>50	>50	>50	>50	4.37
	GM9_TH8	0.011	0.039	0.027	1.50	3.29	>50	0.40	1.39	10.22	0.09

Figure 1. **HIV-1 Env-specific Ab responses and memory B cell repertoire. (A)** Overview of the immunization regimen. Chinese origin rhesus macaques (n = 4, from one independent experiment) were inoculated i.m. six times at weeks 0, 4, 12, 24, 36, and 45 with 16055 Env NFL trimers formulated in the Matrix-M adjuvant. Blood samples were collected before the first inoculation and 2 wk after each inoculation (left). Measurements of the plasma neutralizing titers against the 16055 virus identified D20 as the best responder animal (right; representative data from two independent experiments). **(B)** Single memory B cell sorting 2 wk after the sixth immunization. Approximately 1,000 single Env-specific IgG$^+$ memory B cells were sorted for isolation of Ab HC sequences. For a

subset of the cells, the matching LC was isolated for expression of the corresponding Env-specific mAbs (one independent experiment). **(C and D)** V and J gene assignments. The V and J gene usage of all full-length HC sequences (n = 672) is shown as black bars, with the level of SHM for each Ab sequence shown as superimposed red circles. The average SHM for each V or J gene at the nucleotide level is shown as blue bars. **(E)** Clonality of the Env-specific response. Applying a definition of clonal relatedness as HC sequences with the same V and J gene assignments, identical HCDR3 length and 80%* HCDR3 sequence identity to the 672 HC sequences (red bar) resulted in the identification of 180 Env-specific clonotypes (pink bar). **(F)** Genetic characteristics and IC_{50} neutralizing titers of Env-specific mAbs. Of the 17 cloned Env-specific mAbs, three neutralized the tier 2 isolate 16055, with the GM9_TH8 mAb being most potent (data from one independent experiment). **(G)** Binding of the biotinylated GM9_TH8 mAb to the 16055 NFL trimers (His-captured) in the presence of nonbiotinylated mAb competitors measured by ELISA. The GE136 mAb, a non–broadly neutralizing CD4bs-directed Ab (Sundling et al., 2012a), was used as a negative control (representative data from duplicate wells from two independent experiments). The trimer crystal structure (PDB: 5FYJ) shows the approximate epitope locations of the various mAbs as indicated. Residues corresponding to the V2b loop are shaded in magenta. **(H)** GM9_TH8 and b6 binding to 16055 gp120 and to a variant of gp120 lacking the V2b region (ΔV2b) as measured by ELISA. **(I)** Epitope specificity of the D11A.F2 and GM9_TH8 mAbs as measured by neutralizing activity (IC_{50}, μg/ml) against a panel of Ala mutants along the V2b region compared with WT 16055. Mutations resulting in a significant loss of neutralization capacity (>30-fold) are shaded in gray.

Using the 80%* criterion, we defined 180 clonal Ab lineages among the 672 HC sequences (Fig. 1 E), with HCDR3 lengths ranging from 5 to 24 aa. There was one highly expanded clone in the single-cell data with an HCDR3 of 7 aa: GM4_TD7. The large representation of this clonal family, composed of 84 variants, was apparent when comparing the HCDR3 length distribution of the starting 672 HC sequences with that of the 180 clonotypes defined by the 80%* criterion (Fig. S1 D).

To confirm the specificity of the FACS sorting, we picked the GM4_TD7 HC sequence and 20 additional HCs from families displaying varying levels of expansion and isolated their matching light chain (LC) VJ sequences from the originally single sorted cells. Expression of the resulting mAbs demonstrated that 17 of 21 were Env-specific by ELISA, including GM4_TD7 (Fig. S1 E). Three mAbs, GM9_TH8, GM3_TC2, and GM6_TG1, neutralized the autologous tier 2 16055 virus, while GM7_TE9 and GM7_TH2 neutralized the MW965 isolate, and the remaining mAbs were non-neutralizing (Fig. 1 F). The most potent 16055-neutralizing mAb, GM9_TH8, was ∼100-fold more potent than the previously reported D11A.F9 and D11A.F2 mAbs (Martinez-Murillo et al., 2017). To determine if the GM9_TH8 mAb recognized a similar V2 epitope as the D11A.F2 mAb, we performed cross-competition ELISAs (Fig. 1 G). The results demonstrated that the two Abs competed efficiently with each other, while they did not compete with PGT145 (trimer apex), VRC01 (CD4bs), or 3BC315 (gp41 interprotomeric). We also performed a subtractive binding assay using 16055 gp120 with or without a deletion in the V2b region (gp120ΔV2b) targeted by the D11A.F2 mAb, which showed that GM9_TH8 was able to bind gp120 but was unable to bind the ΔV2b protein. The control mAb, b6, which recognizes the CD4bs, bound gp120 and gp120ΔV2b equivalently (Fig. 1 H). Finally, we compared the fine epitope specificity of D11A.F2 and GM9_TH8 by performing a neutralizing assay using viruses carrying individual alanine substitutions across the V2b region. This revealed that GM9_TH8 bound a similar but not identical epitope in the V2b region, perhaps in part explaining its increased potency compared with D11A.F2 (Fig. 1 I). We performed further ELISA binding assays to map additional mAbs and found that three of the non-neutralizing mAbs, GM5_TF7, GM11_TG8, and GM9_TH5, bound the 16055 gp140 trimers but not the 16055 gp120 monomers, suggesting that they were directed against gp41 (Fig. S1 E). The two 16055-neutralizing mAbs, GM3_TC2 and GM6_TG1, bound WT gp120 and gp120ΔV1, but did not bind gp120ΔV1V2 or gp120ΔV2b, demonstrating that they had similar epitope specificity as GM9_TH8. In contrast, the MW965-neutralizing mAb, GM7_TH2, bound all four gp120 ligands (WT gp120, gp120ΔV1, gp120ΔV1V2, and gp120ΔV2b), and it also bound the 16055 V3 peptide, demonstrating that it was V3-specific (Fig. S1 E). The remaining non-neutralizing mAbs that recognized gp120 were not further mapped.

VH gene usage in the different immune compartments was similar

In addition to the peripheral blood sample used for Env-specific FACS sorting and mAb isolation, we collected BM, spleen, draining inguinal LN (iLN), and ileum lymphoid tissue (gut) from the post-6 termination time point for library constructions and Rep-seq analysis of animal D20 (Figs. 2 and 3). In addition, libraries from blood post-1, post-2, and post-4 time points (Fig. 4) and BM post-2 and post-4 time points (Fig. S3 B) were generated for longitudinal analysis of Env-specific lineages. To establish baseline information, we sequenced the post-6 total IgG repertoire from each compartment and defined the frequencies of V and J gene usage in each library. We assigned all IgG HC sequences with unique bar codes (see Materials and methods) to the individualized germline V gene database of D20 and observed abundant usage of some germline genes and moderate-to-low frequency usage of others. There was no marked difference in V gene usage in the overall IgG repertoires in the different compartments compared with in the pre-immunization blood IgM repertoire (Fig. 2 B). The similarity in V gene usage between the pre- and postimmunization samples is consistent with previous data showing that Env vaccine-induced responses comprise a minor fraction of the total memory B cell repertoire 2 wk after immunization, once the short-lived plasma cell response has declined (Martinez et al., 2015; Sundling et al., 2010). The results were similar for the J genes, with no detectable difference in gene usage between the compartments or between pre- and postimmunization samples (Fig. 2 C).

The Rep-seq library statistics, including numbers of reads, merged reads, barcode clusters, unique VDJ sequences, and numbers of clonotypes (Fig. 2 D), confirm the deep sampling of the B cell repertoire from each compartment. The clonal diversity in the BM was notably lower than that observed in the other compartments, perhaps reflecting a more stringent selection process for B cells to access this compartment. When comparing the HCDR3 lengths of the clonotypes identified in the five

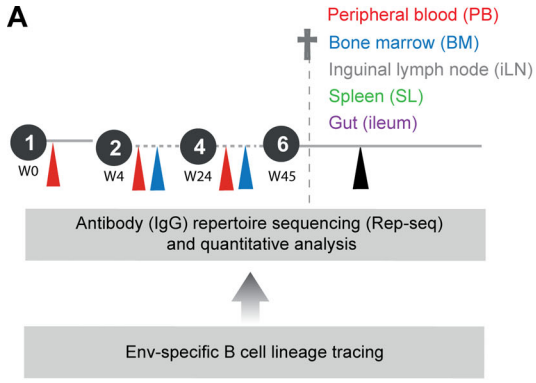

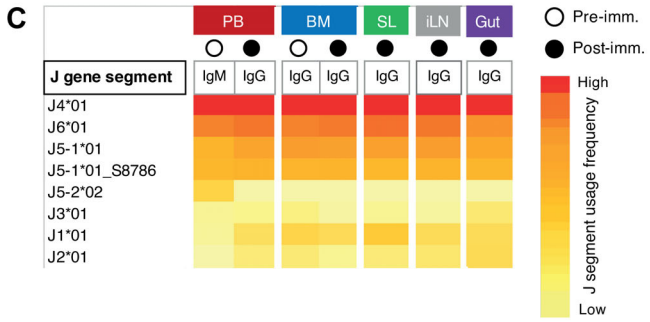

D

Compartment	Total reads	Merged reads	Barcode clusters	Unique VDJ sequences	Clonotypes
Peripheral blood (PB)	3,546,531	3,394,147	1,698,475	1,518,699	123,228
Bone marrow (BM)	2,075,949	2,069,047	1,502,513	1,436,401	23,448
Inguinal lymph node (iLN)	2,874,018	2,750,523	2,033,643	1,858,215	98,553
Spleen (SL)	2,550,419	2,460,066	1,853,760	1,696,492	84,926
Gut (ileum)	3,777,056	3,673,339	2,086,307	1,915,650	109,472

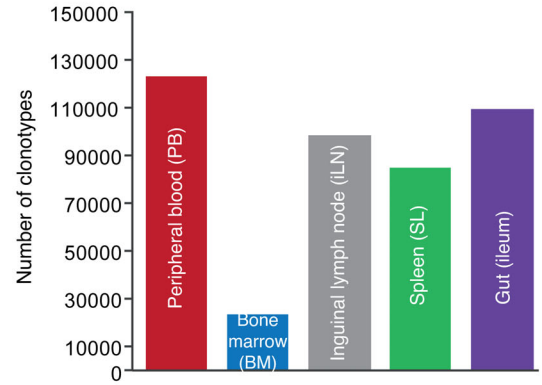

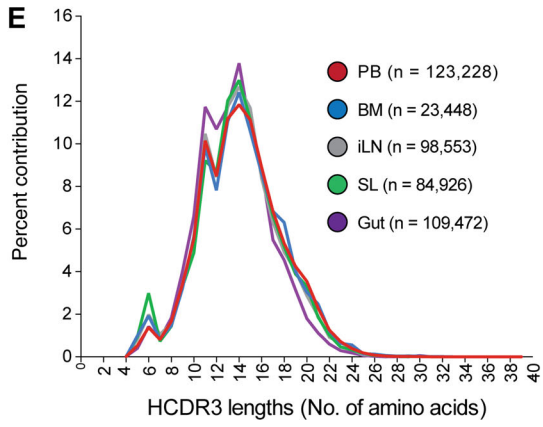

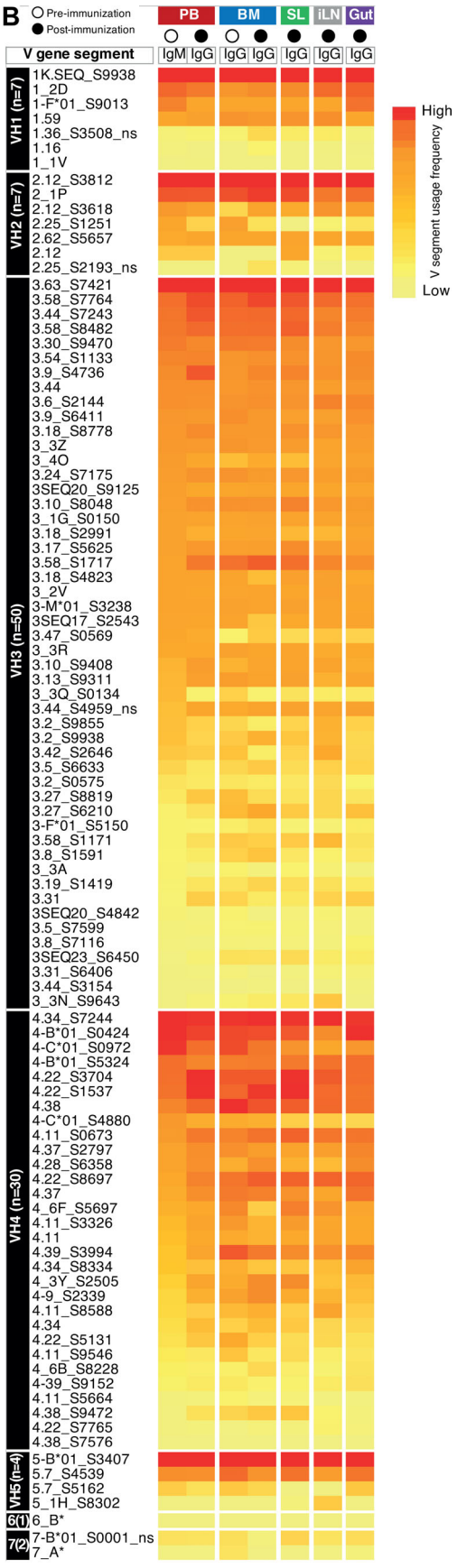

Figure 2. **VH and JH gene usage and clonality of Ab repertoires in different immune compartments. (A)** Tissue sampling from D20. IgG HC libraries from blood, BM, draining iLN, spleen, and gut (ileum) were constructed and deep sequenced. **(B and C)** After processing, the sequences were assigned to the VH (B) and JH (C) germline alleles identified in the D20 animal. The genes are shown familywise (VH1–VH7), with the most frequently used VH (B) and JH (C) allele in each family, based on the IgM library, at the top. **(D)** Top: Sequencing metadata. Total reads, number of raw sequences generated using the MiSeq 2× 300-bp sequencing platform in libraries made from different tissue compartments; merged reads, number of paired sequences; barcode clusters, number of sequences after collapsing sequences with identical barcodes and HCDR3 into a single consensus sequence (including singletons); unique VDJ sequences, total number of uniquely barcoded in-frame Ab sequences; clonotypes, number of unique clonotypes defined as sequences with the same VH and JH gene assignments, identical HCDR3 length, and 80%* HCDR3 sequence identity, also depicted in the lower panel (data from one independent experiment). **(E)** HCDR3 length distribution shown as the percentage of sequences with a given HCDR3 length of the total number of clonotypes. The Next Generation Sequencing experiment was performed once, and the analyses, at least twice.

compartments, we found a similar length distribution in all compartments analyzed (Fig. 2 E).

Vaccine-induced B cell responses seed multiple immune compartments

The next step in our analysis was to trace the 180 Env-specific lineages in the Rep-seq data generated from the different immune compartments. We used the IgDiscover module Clonoquery (see Materials and methods) to identify clonally related sequences for each given query sequence in the Rep-seq data, using the 80%* criterion to define somatic variants for each Ab lineage. We first investigated how many of the 180 Env-specific lineages isolated from circulating memory B cells could be detected in the BM, spleen, or gut lymphoid tissue, and we also probed the draining LN, which we expected would contain abundant vaccine-induced Ab sequences. Lineage tracing identified more than half of the Env-specific Ab lineages in both the draining LN and spleen, consistent with ongoing germinal center (GC) responses in these compartments 2 wk after boosting as we previously reported using a similar immunization regimen (Martinez-Murillo et al., 2017). We detected several vaccine-induced Ab lineages in the BM, perhaps representing plasma cells destined to persist as long-lived cells. In contrast, we could not trace many Env-specific Ab lineages in the ileum, suggesting limited dissemination to this compartment following i.m. vaccine inoculation. Overall, the numbers of traced Ab lineages were 101 (56%) in blood, 111 (62%) in draining LN, 102 (57%) in spleen, 41 (23%) in BM, and 8 (<5%) in ileum (Fig. 3 A).

The level of expansion varied significantly between the lineages. Some were represented by hundreds of variants in the Rep-seq data and detected in all compartments, while other lineages were represented by only a few variants in selected compartments, and other lineages were not detected at all. We sorted for Env-binding memory B cells, but a fraction of the lineages may be nonspecific, as shown by the recognition profiles displayed by the isolated mAbs (17 of the 21 cloned Abs were Env specific), potentially explaining the lack of expansion for a subset of the lineages following boosting. The non-neutralizing GM4_TD7 lineage, which we already identified as an expanded clone from our single-cell data, was highly expanded, as were the GM2_TD2 and GM9_TH5 lineages (Fig. 3 B). One 16055-neutralizing lineage, GM6_TG1, was represented by many somatic variants in BM, while the more potent 16055-neutralizing lineage, GM9_TH8, could not be traced in BM.

For an independent confirmation that Env-specific B cells were present in the different compartments, we analyzed the samples by B cell ELISpot assay using two distinct protocols that enumerate memory B cells and plasma cells, respectively. We demonstrate that Env-specific memory B cells were abundant in blood, draining LN, and spleen but undetectable in BM and ileum (Fig. S3, left). In contrast, Env-specific plasma cells were present in BM, draining LN, and spleen but undetectable in blood and ileum (Fig. S3, right). These results are consistent with our previous observations that short-lived antigen-specific plasma cells are no longer present in blood 2 wk after boosting and that the BM compartment does not harbor vaccine-induced memory B cells (Sundling et al., 2010). Based on the ELISpot results, our interpretation is that the variants traced in the blood represent memory B cells, while the variants traced in the BM represent plasma cells. Whether these Env-specific plasma cells represent long-lived plasma cells could not be determined with the sampling time points used in the current study. The spleen and LN harbored both antigen-specific memory B cells and plasma cells, consistent with ongoing GC responses in these compartments.

When analyzing V region SHM levels of all variants belonging to a unique Ab lineage, i.e., intraclonal analysis, for a large set of Env-specific lineages, we found that the most highly mutated variants were present in the draining LN and spleen, again consistent with ongoing GC reactions in these compartments at this time point (Fig. 3 C). Because the post-6 time point was the termination time point, we could not determine if these variants eventually entered the circulation. However, these data demonstrate the capacity of the immune system to promote multiple independent vaccine-induced Ab lineages simultaneously after boosting, of which many disseminate to distant immune compartments, including to the BM.

Intraclonal analysis demonstrates increasing SHM in both CDRs and FRs following boosting

We next used Clonoquery to interrogate longitudinal Rep-seq data from animal D20. We used libraries generated from blood collected 2 wk after the second, fourth, and sixth immunizations (post-2, post-4, and post-6). We first determined the level of expansion over time, focusing on 60 of the 180 lineages that we detected most readily in blood (Fig. 4 A). Of these, some lineages increased over time, while others did not. The potent neutralizing Ab lineage GM9_TH8 was among the least expanded, with clonal variants detected only in post-2 and post-6, but not post-4, Rep-seq data. When analyzing SHM levels for individual variants and comparing them intraclonally, we found a gradual increase both between the post-2 and post-4 time points and

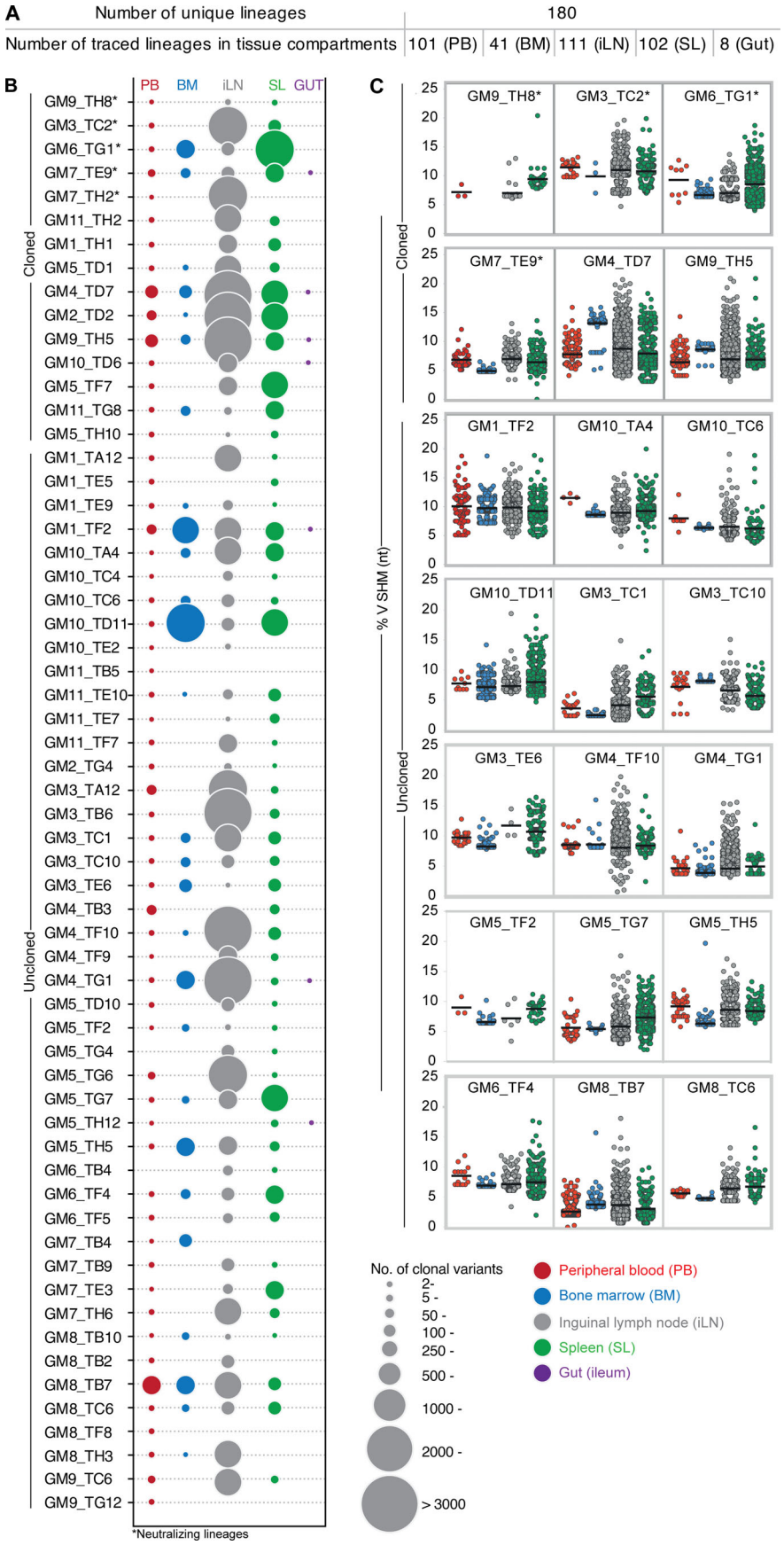

Figure 3. **Clonal expansion, dissemination, and SHM at the post-6 time point in different immune compartments. (A)** Number of variants traced in each immune compartment, defining a lineage as successfully traced when at least two clonally related variants were identified in the Rep-seq data (data from one independent experiment). **(B)** Bubble plot showing the relative distribution and expansion of Env-specific B cell lineages in blood (red), BM (blue), draining iLN (gray), spleen (green), and gut (ileum; purple). The sizes of the bubbles correspond to the number of somatic variants identified for each lineage (data from one independent experiment). **(C)** Intraclonal analysis of SHM shown as percentage divergence from the assigned germline V gene sequence at the nucleotide level. Each box shows one clonal lineage, with each variant of the lineage identified in the Rep-seq represented as one dot (data from one independent experiment). Data from Rep-seq libraries generated from blood (red), BM (blue), draining iLN (gray), and spleen (green). The experiment was performed once, and the analyses, at least twice.

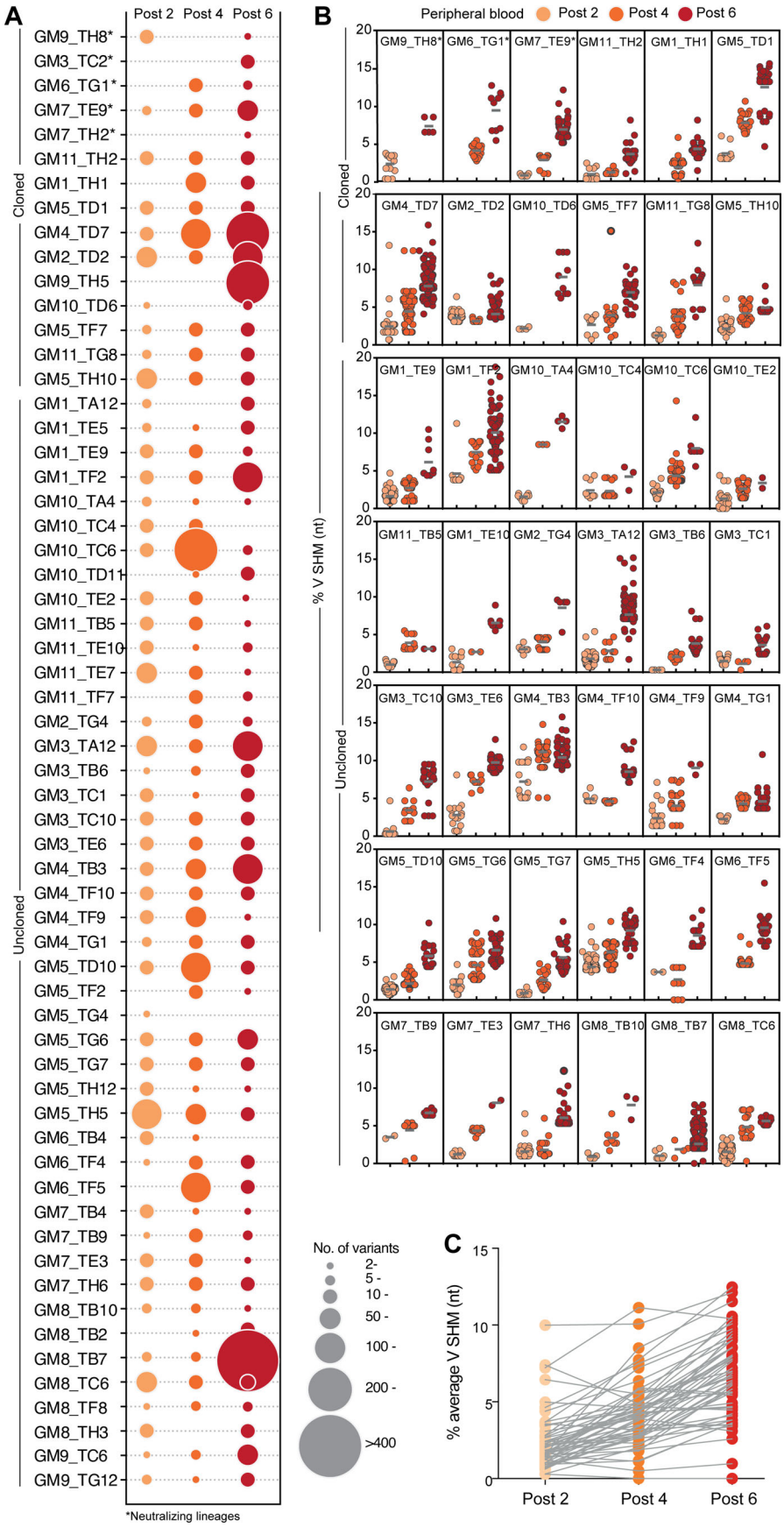

Figure 4. **Clonal expansion, dissemination, and SHM at different time points. (A)** Bubble plot showing the relative expansion of representative Env-specific B cell lineages in Rep-seq data generated from blood after the second, fourth, or sixth immunizations. The sizes of the bubbles correspond to the number of somatic variants identified for each lineage (data from one independent experiment). **(B)** Intraclonal analysis of SHM shown as percentage divergence from the assigned germline V gene sequence at the nucleotide level. Each box shows one clonal lineage, with each variant of the lineage identified in the Rep-seq represented as one dot. Data from Rep-seq libraries generated from the blood post-2, post-4, and post-6 time points (data from one independent experiment). **(C)** Average V region SHM of all the variants identified at the different time points per Ab lineage. The experiment was performed once, and the analyses, at least twice.

between the post-4 and post-6 time points for most lineages, independent of their level of expansion. These data suggest an efficient affinity maturation process for a large number of lineages simultaneously in response to boosting (Fig. 4 B), an effect also observed when plotting the average SHM for all lineages traced in the post-2, post-4, and post-6 Rep-seq data (Fig. 4 C). For the lineages we could trace at more than one time point in the BM, we also observed higher levels of SHM at the post-6 time point compared with the post-2 or post-4 time point (Fig. S3 B), suggesting an active recruitment of affinity-matured variants into this compartment.

Evaluation of average SHM levels across the V gene offers only a rough estimation of the Ab affinity maturation process. For a more detailed analysis, we investigated which region of the Abs accumulated most mutations by calculating average SHM frequencies in the Ab FRs (FR1, FR2, and FR3) and the CDRs (CDR1 and CDR2). The results demonstrated that for most lineages, SHM predominantly accumulated in the CDR2, followed by the CDR1. Interestingly, many lineages also accumulated high SHM levels in FR3 and, in some cases, also in FR2 (Fig. 5 A). To examine this in more detail, we selected 10 lineages for which we identified the unmutated, or close to unmutated, precursor VDJ sequence in the Rep-seq data. This allowed us to assess SHM levels also in the HCDR3, which otherwise is difficult due to ambiguities in the nontemplated VD and DJ junctions. One caveat remained, since our criterion for clonality, 80%*, limits the number of mutations tolerated in the HCDR3. Thus, the SHM levels calculated for this region may be an underestimation. For each of the 10 lineages, we identified nine somatic variants from blood, ranging from low to high SHM, which we aligned with the corresponding precursor sequence to inspect region-specific SHM. This analysis suggested an accumulation of immunization-induced mutations in the CDRs but, in the more mutated variants, also extended to the FRs (Fig. S4). When we plotted the region-specific SHM against the overall SHM for the respective VDJ regions, we observed a clear increase in SHM in the FR3s with increasing SHM in the overall VDJ sequence for all 10 lineages (Fig. 5 B). These results suggest that SHM in multiple Ab regions, including FR2 and FR3, contributes to enhance antigen binding.

SHM levels directly impacts HIV-1 Ab neutralizing capacity

We next selected the GM9_TH8 lineage to functionally test if increases in SHM conferred improved Ab binding and neutralization. We selected 11 HCs, in addition to the HC of the cloned GM9_TH8 mAb, with levels of SHM ranging from 0 to 24% at the amino acid level. Of these HC sequences, we identified one variant with no SHM in the V gene and only one mutation in the J gene in a Rep-seq library following a single Env trimer inoculation. This sequence likely represented the germline GM9_TH8 HC, except for a J gene mutation, which allowed definition of the HCDR3 junctions. We also selected one GM9_TH8 variant from the post-2 BM sample (7.4% SHM), one variant from the post-4 BM sample (16.7% SHM), and several variants from the draining LN and spleen (15.6–24% SHM) collected at post-6 (termination) time point. The amino acid alignment of the 12 HC sequences demonstrated that most of the mutations in the low-SHM variants were located in the HCDR2. In the HCs with higher overall SHM levels, mutations additionally accumulated in the other Ab regions, especially in FR3 (Fig. 6 A). To analyze the relatedness of these 12 GM9_TH8 variants in the context of all traced GM9_TH8 variants from all compartments, we generated a maximum-likelihood tree. The unmutated common ancestor sequence of the tree was created using the assigned germline V and J, with the junction and D gene masked with ambiguous ("N") nucleotides, which are treated as uninformative "missing data" in the phylogenetic likelihood calculation. The resulting tree revealed multiple subbranches, with the GM9_TH8 mAb sequence clustering most closely with variants from the draining LN (Fig. 6 B).

We cotransfected the 12 GM9_TH8 HC sequences with the original GM9_TH8 LC sequence and expressed each variant as both IgG and Fab. We performed ELISAs with or without a NaSCN wash to examine the relative binding avidity of the IgG variants. When the wash was performed in PBS, we observed that the post-1 GM9_TH8 variant (PB_seq681430_post-1), for which the V gene was in the germline configuration, bound the 16055 NFL trimers only weakly, while all other variants, ranging from low SHM to higher, displayed similar binding avidity (Fig. 6 C, left). In contrast, when the ELISA was performed under high salt conditions using a NaSCN wash (Fig. 6 C, right), we observed a marked reduction in binding for the post-2 GM9_TH8 variant (PB_seq24927_post-2), which had seven mutations in the V gene (7.3% SHM), while the more mutated variants of the lineage mostly retained their binding.

For an independent assessment of functionality, we measured the neutralization capacity for both bivalent IgG and monovalent Fabs for each expressed variant of the GM9_TH8 lineage. The post-1 variant of GM9_TH8 (PB_seq681430_post-1), with an unmutated V gene, lacked neutralizing capacity as both IgG and Fab, while all other variants displayed potent tier 2 neutralizing activity as bivalent IgG, including the modestly mutated PB_seq24927_post-2 variant. In contrast, the post-2 variant was only weakly neutralizing as a monomeric Fab (Fig. 6 D). By comparing the monomeric Fab to the bivalent IgG concentration resulting in 50% virus neutralization (IC_{50}) values on a molar basis, it was clear that there was a large effect of avidity on the neutralization potency for this lineage (Figs. 6 D and S5 A). When examining the relationship between SHM and virus neutralization potency for the respective Fabs, we observed a strong correlation for both IC_{50} and IC_{80} with the level of SHM (Fig. 6 E). The most highly mutated variant of GM9_TH8 identified in the Rep-seq data, iLNG_seq732127, displayed 24% SHM at the amino acid level and was the most potent neutralizing Ab of the GM9_TH8 variants analyzed here. We named this variant Ab GM9_TH8seq732127 and obtained crystals of this Fab that diffracted x rays to a 2.26-Å resolution. We used this structure to visualize the location of the amino acid residues modified by SHM. We first analyzed SHM that were common between the GM9_TH8 and GM9_TH8seq732127 HC, which included 2 aa in the HCDR2 (Fig. 6 F, left). We then evaluated SHM that were located at the same position but changed relative to the V gene germline sequence to a different amino acid residue in GM9_TH8 (first letter) compared with GM9_TH8seq732127

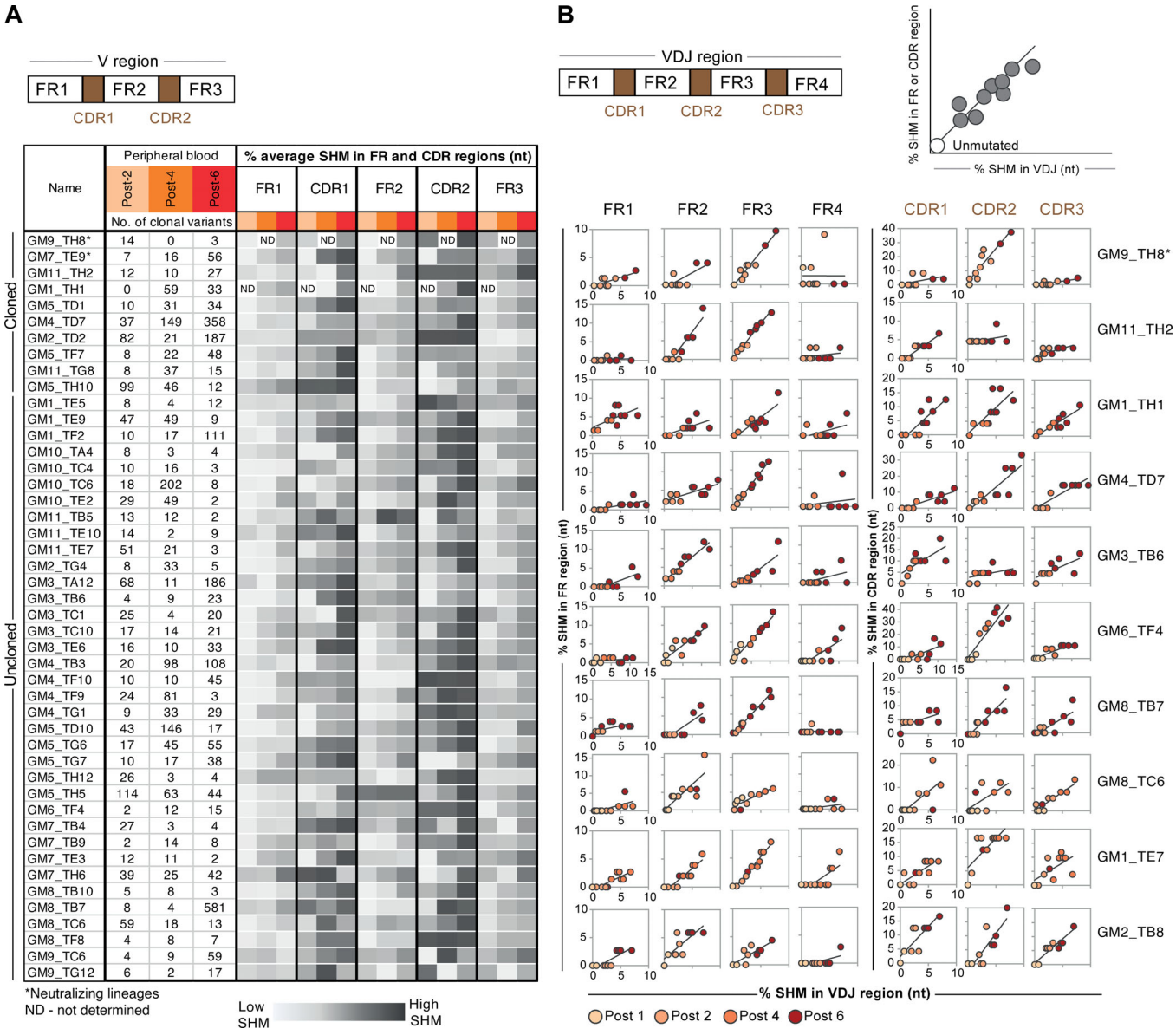

Figure 5. **SHM in FRs and CDRs. (A)** Representative Env-specific lineages traced in the Rep-seq data generated from the blood post-2, post-4, and post-6 time points, with the number of identified somatic variants for each lineage indicated. The columns labeled FR1, CDR1, FR2, CDR2, and FR3 denotes the different subregions of the Ab V region. For every lineage, the percentage average SHM (nucleotide level) for each subregion was calculated from the number of variants identified at a given time point. The percentage average SHM for a given subregion from different time points is indicated with different shades, where darker and lighter gray correspond to higher and lower SHM levels, respectively (representative data from one independent experiment analyzed at least twice). **(B)** SHM (nucleotide level) in subregions (FR1–4 and CDR1–3) plotted relative to the total SHM in the corresponding full VDJ region (upper right schematic) for lineages where unmutated, or close to unmutated, sequences were identified in the Rep-seq data. Ten variants ranging from low to high SHM levels are shown for each lineage (representative data from one independent experiment analyzed at least twice).

(second letter; Fig. 6 F, middle). Finally, we denoted all SHM in the GM9_TH8seq732127 HC to visualize the full spectrum of SHM in this Ab HC (Fig. 6 F, right). At the present time, we do not possess a high-resolution structure of the GM8_TH9 lineage Ab with its epitope on the HIV-1 trimeric spike. Therefore, we cannot draw firm conclusions about direct paratope:epitope contacts. However, the analysis performed here suggested that most SHM, including the mutations in the FR3, affected solvent-exposed residues clustered near the HCDR2, which could be involved in GM9_TH8 recognition of its cognate epitope.

Discussion

Immunization with complex multiepitope proteins results in diverse repertoires of affinity-matured Abs. For HIV-1, the elicitation of protective Abs through vaccination is extremely challenging due to the host-selected *N*-glycan shield that occludes neutralizing epitopes on the native Env spike (Kwong et al., 2002; Wei et al., 2003). How individual antigen-specific Env-specific B cell lineages evolve following immunization is a subject of recent interest (Cirelli et al., 2019; Luo et al., 2016; Wang et al., 2016; Yacoob et al., 2018), which we address here at

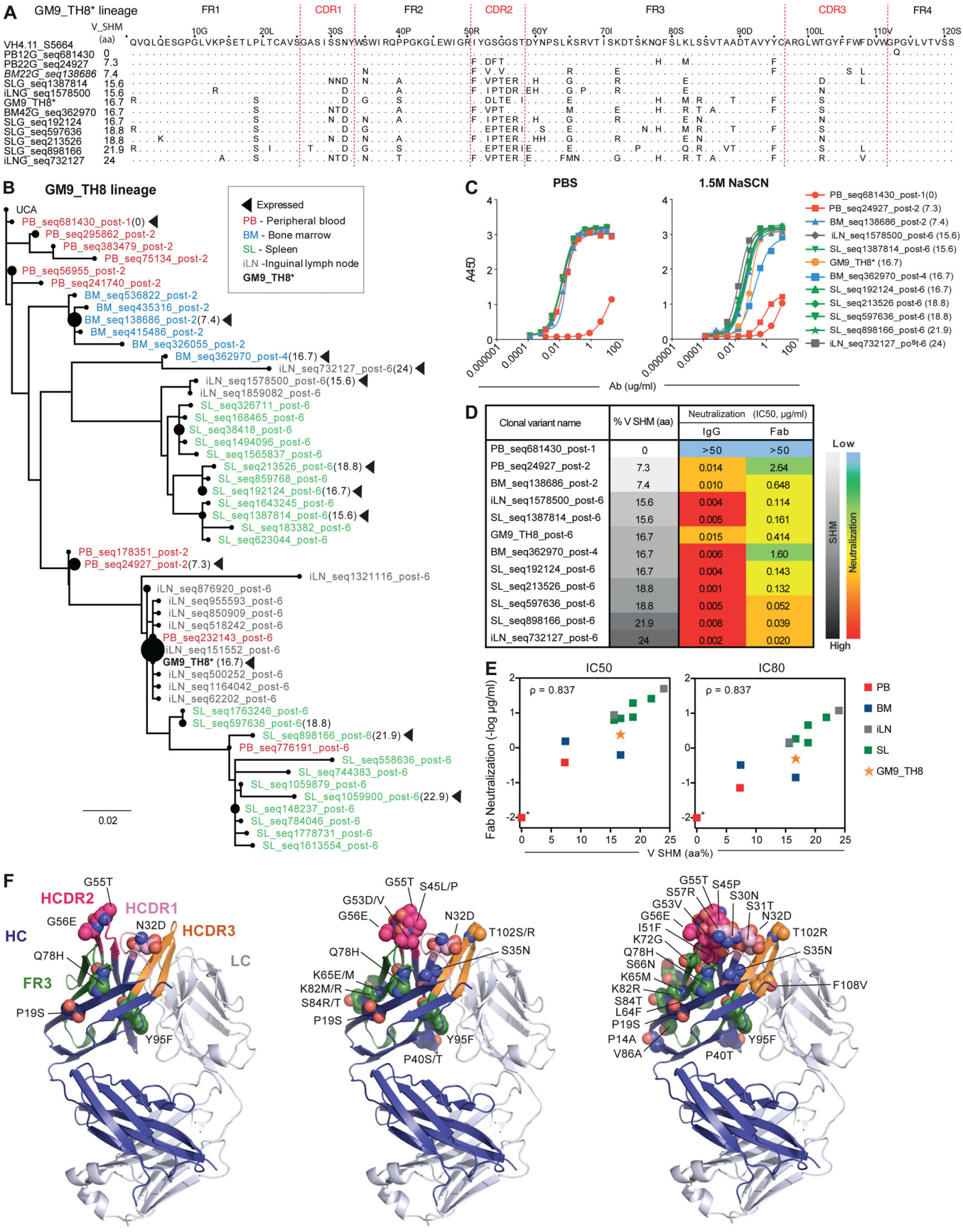

Figure 6. **Impact of SHM on the neutralizing capacity of GM9_TH8 lineage. (A)** The alignment of 11 HC somatic variants of GM9_TH8 lineage selected from multiple immune compartments, in addition to the HC of cloned GM9_TH8 mAb, with levels of SHM ranging from 0 to 24% at the amino acid level. The top row shows the inferred germline sequence of HC, where the VD and DJ junctions were determined based on the least-mutated variant found in the blood Rep-seq data. **(B)** Maximum likelihood phylogenetic tree showing HC sequences from the GM9_TH8 lineage with the 12 expressed GM9_TH8 variants (representative data from two independent experiments) indicated with arrows. **(C)** Binding curves for each of the 12 GM9_TH8 variants analyzed in conventional ELISA (PBS) or in the presence of high salt (NaSCN; representative data from duplicate wells from two independent experiments). **(D)** Autologous tier 2 neutralizing activity of the 12 GM9_TH8 variants as IgG or Fab shown in the order of increasing SHM (data from one independent experiment). **(E)** Scatter plots of SHM versus Fab neutralizing activity (IC_{50} or IC_{80}) were generated, and the Spearman rank correlation coefficient (ρ) was computed using Prism software (GraphPad, v7; ρ = 0.837). Asterisk indicates that the non-neutralizing PB_seq681430_post-1 Ab was assigned IC_{50} and IC_{80} values of 100 for the purpose of the calculation. Data points are color-coded according to compartment. The analyses of Ab function were performed twice. **(F)** Representation of the GM9_TH8seq732127 Fab structure. LC is shown in light blue/gray and HC in dark blue, with HCDR1 in pink, HCDR2 in magenta, HCDR3 in orange, and FR3 in green. Mutated residues are shown in spheres and labeled. Left: Shared SHM between the GM9_TH8 HC and the GM9_TH8seq732127 HC. Middle: SHM at the same position but mutated to a different aa residue for GM9_TH8 (first letter) compared to GM9_TH8seq732127 (second letter). Right: All SHM in the GM9_TH8seq732127 HC.

a comprehensive level. This aspect is important to understand to design improved vaccine regimens against pathogens for which vaccines do not yet exist.

Previously, we demonstrated that the well-ordered 16055 NFL trimers elicit autologous neutralizing Abs in rhesus macaques that target a region of the Env trimer apex (Martinez-Murillo et al., 2017). As also observed here, boosting did not significantly increase the titers of the neutralizing Ab response, suggesting restricted affinity maturation or poor persistence of the responding B cell clones over time. Here, we traced Env vaccine-induced Ab HC sequences in Rep-seq data to determine how individual Ab lineages evolved in response to trimer boosting. We demonstrate that even poorly expanded Ab lineages accumulated high levels of SHM following boosting, as we observed for the GM9_TH8 lineage. These data indicate that affinity maturation per se is not the limiting factor for the neutralizing Ab response, suggesting that it is the frequency of naive B cells capable of recognizing neutralizing Ab epitopes, and/or the level of expansion of such B cell lineages, that limits the development of effective neutralizing responses. While several clones likely contributed to the plasma neutralizing response, the other 16055-neutralzing Abs isolated here, GM3_TC2 and GM6_TG1, were markedly less potent than GM9_TH8. Furthermore, as observed in this study and in previous studies aimed at isolating Env vaccine-induced mAbs (Martinez-Murillo et al., 2017; Phad et al., 2015), typically only a small fraction of the total number of isolated mAbs are neutralizing. Here, we additionally find that several non-neutralizing mAbs, such as GM4_TD7, displayed a significantly greater level of expansion following boosting compared with the neutralizing Ab lineages traced here.

As expected, SHM accumulated primarily in the HC CDRs and in particular the CDR2; although as expected, each lineage was unique in its SHM pattern. In variants with high overall levels of SHM, mutations also accumulated in the FR3 and to a lesser extent in the FR2. High levels of SHM in Ab FRs has been described as a feature selectively detected in chronically HIV-infected individuals (Klein et al., 2013), but we show here that this can also occur in response to vaccination. The high levels of SHM (24% at the amino acid level) that can accumulate in members of given Ab lineages, affecting both CDRs and FRs, are encouraging, especially regarding the elicitation of HIV-1 neutralizing Abs following sequential Env trimer vaccination. Although we cannot determine definitively which SHM observed in the GM8_TH9 lineage are direct contacts with the cognate Env trimer antigen (some may be neutral or affect Ab stability), that such levels can occur following sequential subunit immunization and result in improved binding and neutralizing Abs is encouraging for future vaccine efforts. Together, these are important observations, since high levels of SHM are displayed by many HIV-1 broadly neutralizing Abs derived from chronic infection and long-term antigen exposure.

Our results demonstrate broad compartmental dissemination of the vaccine-elicited Ab lineages in draining LN, blood, spleen, and BM. Previously, we demonstrated active GC responses in draining LN 2 wk after inoculation with NFL Env trimers administered in Matrix-M adjuvant, also used here (Martinez-Murillo et al., 2017). The presence of GCs at this time point is consistent with the lineage-tracing analyses presented here, which identified hundreds to thousands of somatic variants for each Env-specific lineage in the draining LN and spleen, and considerably fewer somatic variants for each lineage in blood and BM. This is also consistent with the B cell ELISpot analysis reported here, which demonstrates the copresence of Env-specific memory B cells and plasma cells in the draining LN and spleen, where plasma cells likely contributed a greater total number of sequences to the Rep-seq data due to the high copy number of Ab transcripts in these cells. In contrast, we detected only memory B cells in blood and only plasma cells in the BM, which we interpret to represent the GC output. We did not detect Env-specific B cells in the ileum despite high numbers of total IgG memory B cells and plasma cells in this compartment, in agreement with a previous vaccination study (Luo et al., 2016) and a study of total B cell repertoires in humans, demonstrating limited exchange between the gut and peripheral blood B cell repertoires (Meng et al., 2017). This finding, however, does not rule out that soluble IgG induced by i.m. immunization diffuses to mucosal sites, including to the gut, to mediate protective effects in these anatomic sites.

The use of the IgDiscover germline gene inference tool (Corcoran et al., 2016) generated a robust foundation for the precise genetic analyses and lineage-tracing studies reported here. To accomplish nucleotide-level precision, an individualized database is required due to the high allelic diversity in

rhesus macaques (Shen et al., 2013) and the lack of a comprehensive public database for macaque Ab germline genes. Our current understanding of the concordance between the peripheral memory B cell compartment and the BM plasma cell compartment is limited. The methodological approach described here offers possibilities to investigate this further. For example, it would be of interest to apply the analysis approach used here, combining single-cell sequencing and mAb isolation with Rep-seq, to elucidate if different modes of vaccination (Cirelli et al., 2019) alter the developmental pathways of vaccine-induced Ab lineages targeting distinct epitopes of Env.

In conclusion, the current study offers a comprehensive, in-depth analysis of the evolution of Ab responses following immunization with well-ordered HIV Env trimers. This study investigates and, to some extent, defines the process of Ab affinity maturation and dissemination of B cells to selected immune compartments. Elucidating the Env-specific polyclonal response at great depth, as performed here, improves our understanding of vaccine-induced responses and provides a basis for future efforts to design more effective immunization regimens.

Materials and methods

Animals

Four female rhesus macaques (*Macaca mulatta*) of Chinese origin, 4–10 yr old, were housed at the Astrid Fagraeus Laboratory at Karolinska Institutet. Housing and care procedures complied with the provisions and general guidelines of the Swedish Board of Agriculture. The facility has been assigned an Animal Welfare Assurance number by the Office of Laboratory Animal Welfare at the National Institutes of Health. The macaques were housed in pairs in 4-m^3 cages, enriched to give them ability to express their physiological and behavioral needs. They were habituated to the housing conditions for >6 wk before the start of the experiment and subjected to positive reinforcement training to reduce the stress associated with experimental procedures. All immunizations and blood samplings were performed under sedation with ketamine 10–15 mg/kg i.m. (Ketaminol, 100 mg/ml; Intervet). The macaques were weighed at each sampling. All animals were confirmed negative for simian immunodeficiency virus, simian T cell lymphotropic virus, simian retrovirus type D, and simian herpes B virus.

Ethics statement

The animal work was conducted with the approval of the regional Ethical Committee on Animal Experiments (Stockholms Norra Djurförsöksetiska Nämnd). All methods were performed in accordance with the approved guidelines.

HIV-1 Env immunogens and probes

The design, expression, and purification of clade C 16055 NFL TD CC trimers from transient expression in 293F cells were previously described (Guenaga et al., 2015). In brief, the 16055 Env coding sequence was modified as follows: the native signal sequence was replaced by the CD5 signal sequence, the furin cleavage motif at the C terminus of gp120 was replaced with two copies of the G_4S flexible linker, a K334S mutation was introduced to restore the 332N-glycan supersite, and eight TD modifications were introduced to stabilize trimer formation, along with the previously described I559P, I201C, and A433C substitutions. The sequence was terminated at D664 followed by a G_4S linker and His_6 tag. Cell culture supernatants containing the expressed Env proteins were collected 4–5 d after transfection and purified over a *Galanthus nivalis* lectin-agarose (Vector Laboratories) column followed by size exclusion chromatography to isolate the trimer. For the trimer probe, the His_6 tag was replaced by AviTag and biotinylated with BirA (Avidity).

Immunization and sampling

Animals were inoculated six times at weeks 0, 4, 12, 24, 36, and 45 i.m. in a total volume of 1 ml, divided equally between the left and right quadriceps (100 µg Env formulated in 75 µg Matrix-M adjuvant [Novavax] per inoculation; Sharma et al., 2015). The trimers from the first two inoculations contained 4 *N*-glycan deletions proximal to the CD4bs as previously described (Dubrovskaya et al., 2017). Peripheral blood samples were collected 2 wk after each immunization, and BM aspirates were taken 2 wk after the second, fourth, and sixth immunizations. Tissue samples, including iLN, spleen, and ileum, were collected at termination, i.e., 2 wk after the sixth immunization.

Cell isolation

PBMCs and cells from BM were isolated by density-gradient centrifugation from EDTA blood by Ficoll-Paque PLUS (GE Healthcare), washed extensively in PBS, and treated with red blood cell lysis buffer. Single-cell suspensions of splenocytes and LN cells were prepared using a 70-µm cell strainer and a syringe plunger. Cell suspensions were washed once in Ca^{2+}- and Mg^{2+}-free PBS (Sigma-Aldrich) and treated with red blood cell lysis buffer. Cell samples collected from different immune compartments were frozen in 90% heat-inactivated FBS and 10% DMSO (Sigma-Aldrich). Intestinal lamina propria cells were isolated from duodenum, ileum, or colon tissue of rhesus macaques, as previously described for murine tissue (Parigi et al., 2018). Briefly, 5-cm-long intestinal samples were placed in ice-cold PBS. After removal of residual mesenteric fat tissue, the intestines were opened longitudinally and cut into 1-cm pieces. After extensive washing, tissues were incubated in a shaking incubator at 37°C for 30 min in 20 ml of HBSS containing 5% FCS, 5 mM EDTA, 1 mM dithiothreitol, and 15 mM Hepes. Tissue pieces were washed with 20 ml PBS with 5% FCS and 1 mM EDTA followed by PBS with 1% FCS and 15 mM Hepes. Digestion was performed in 10 ml of serum-free HBSS containing Liberase TL (0.15 mg/ml; Roche) and 0.1 mg/ml DNase I (Roche) at 37°C at 600 rpm for 45 min. Cells were washed and passed through a 100-µm cell strainer. Cells were separated at the interphase of a 44–67% Percoll (Sigma-Aldrich) gradient.

Single-cell sorting of HIV-1 Env-specific memory B cells by flow cytometry

Env-specific memory B cells were single-cell sorted from PBMCs from animal D20 sampled 2 wk after the sixth immunization. Single cells were sorted with a three-laser FACSAria cell sorter (BD Bioscience) by gating Live/Dead stain (Life Technologies)–negative,

$CD3^-$, $CD14^-$, $CD20^+$, IgG^+, $CD27^+$, Env^+ cells into 96-well PCR plates containing 4 µl of cell lysis buffer (Sundling et al., 2012a). Plates were sealed and immediately frozen on dry ice before storage at −80°C. All fluorescently labeled Abs and the biotinylated Env-trimer conjugated to streptavidin-allophycocyanin (Invitrogen) were carefully titrated to stain rhesus macaques PBMCs.

Single B cell RT-PCR

Sorted HIV-1 Env-specific single memory B cells from animal D20 were lysed and reverse transcribed, and VDJ sequences were amplified as described previously (Sundling et al., 2012a,b). Briefly, the 96-well plates containing single B cells, were thawed on ice and reverse transcribed to cDNA by addition of random hexamers, dNTPs, and SuperScript III reverse transcription (Invitrogen). The VDJ sequences were amplified separately in 25-µl nested PCR reactions using 3 µl of cDNA in the first-round PCR and 1.5 µl PCR product in the second-round PCR. The HotStar Taq Plus Kit (Qiagen) and 5′ leader sequence-specific and 3′ IgG-specific primers were used. PCR products from the positive wells were purified, sequenced (GATC Biotech), and analyzed. The productive HC and LC sequences were reamplified in 25-µl cloning PCR reactions to add the cloning sites using 2-µl nested PCR product with Kappa Mix (Kappa Biosystems) and 5′ and 3′ custom cloning primers containing restriction sites previously described (Sundling et al., 2012b; Tiller et al., 2008).

Cloning and expression of mAbs

Cloning PCR products were evaluated on 1% agarose gel for correct size (~450 bp for HC and ~350 bp for κ or λ LC), and then PCR purified. Cloning of the Ab sequences into expression vectors containing human Igγ1 H, Igκ1 liter, or Igλ2 liter constant regions (Tiller et al., 2008) were performed with FastDigest restriction enzymes (Thermo Fisher Scientific) according to the manufacturer's instructions. The digested PCR products were inserted into linearized, shrimp alkaline phosphatase–treated vectors using T4 DNA ligase (Thermo Fisher Scientific). XL10-Gold ultracompetent cells were transformed by heat shock at 42°C for 45 s according to the manufacturer's protocol (Agilent Technologies). Positive colonies were verified for insert by PCR. Bacterial colonies containing plasmids with inserts of the correct size were then expanded, followed by plasmid purification (Qiagen) and Sanger sequencing (GATC Biotech). For Ab expression, 15 µg of each HC and LC vector DNA was transfected into FreeStyle 293-F cells and cultured in 30 ml of FreeStyle 293 expression medium (Life Technologies) at a cell density of 10^6 cells/ml and ≥90% viability, using 30 µl of 293fectin (Life Technologies) according to the manufacturer's protocol. After 4–5 d, cell culture supernatants were tested for total Ab production and for binding to HIV-1 Env ligands by ELISA. Cultures containing functional Env-specific Abs were then harvested and purified 7 d after transfection using Protein G Sepharose columns (GE Healthcare). All purified recombinant mAbs were analyzed by SDS-PAGE under reducing conditions using NuPAGE Novex 4–12% Bis-Tris polyacrylamide gels and NuPAGE reducing agent (Life Technologies) according to the manufacturer's instructions.

HIV-1 neutralization assays

Neutralization assays were performed using a single-round infectious HIV-1 Env pseudovirus assay with TZM-bl target cells (Li et al., 2005). To determine the Ab concentration and the plasma dilution that resulted in a 50% reduction in relative luciferase units, serial dilutions of the mAbs and the plasma were performed, and the neutralization dose–response curves were fitted by nonlinear regression using a five-parameter Hill slope equation using the R statistical software package. Neutralization capacities of mAbs were reported as the Ab IC_{50}, whereas the results for plasma were reported as the plasma neutralization ID_{50}, which is the reciprocal of the plasma dilution producing 50% virus neutralization.

ELISA for Env binding

The mAbs were tested for binding against 16055 NFL TD CC trimer, gp120, and the gp120 V2b(180–194) deletion mutant with residues replaced with GAG (Martinez-Murillo et al., 2017). MaxiSorp 96-well plates (Nalgene Nunc International) were coated at 2 µg/ml with WT gp120, gp120 V2b, or with an anti-His tag mAb (AD1.1.10; R&D Systems) to capture the His-tagged trimer in PBS at 4°C overnight. After incubation with blocking buffer (PBS containing 2% nonfat milk), the mAbs were added and incubated for 1 h at 37°C. Binding was detected by secondary HRP-conjugated anti-human Fcγ Ab (Jackson ImmunoResearch) at 1:10,000 for 1 h. The signal was developed by addition of TMB substrate (Invitrogen) for 5 min, reactions were terminated with 1 N sulfuric acid, and the OD was read at 450 nm. Between each incubation step, the plates were washed six times with PBS containing 0.05% Tween-20.

Cross-competition ELISA

GM9_TH8 was biotinylated using EZ-Link NHS-Biotin (Pierce Biotechnology, Thermo Fisher Scientific) per the manufacturer's protocol. For cross-competition ELISA assays, 16055 NFL TD CC trimers were captured on the ELISA plate by an anti-His tag mAb (R&D Systems) coated at 2 µg/ml in PBS at 4°C overnight. Fivefold serial dilutions of competing mAbs were preincubated with the captured trimer at RT for 30 min before addition of biotinylated GM9_TH8 at a concentration previously determined to give ~75% of the maximum binding signal (i.e., binding to trimer with no competitor present) for 60 min at RT. The bound biotinylated mAbs were detected using HRP-conjugated streptavidin (Sigma-Aldrich). The signal was detected with tetramethylbenzidine substrate, and the reaction was stopped with 1 N sulfuric acid. Wells were blocked with 5% nonfat milk in PBS-T (0.2% Tween-20) after coating with the anti-His mAb and washed with PBS-T after each incubation step. Samples were diluted in 10% blocking buffer.

Avidity ELISA

The GM9_TH8 lineage mAbs were assessed by a chaotropic ELISA wash assay using sodium thiocyanate (NaSCN). An additional wash incubation step with PBS or 1.5 M NaSCN was included after Ab binding to the His-captured 16055 NFL TD CC trimers. Binding of the mAbs was detected after incubation with the HRP-conjugated secondary Ab as described above.

GM9_TH8 lineage IgG and Fab Expression

The HCs from the selected clones were paired with the GM9_TH8 LC, expressed by transient transfection into 293F cells, and purified as described above. For Fab expression, the VDJ segments were cloned into the Fab expression vector, which contains stop codons in the HC hinge region (EPKSCDK**). All constructs were sequence verified. Similarly, each Fab HC was paired with the GM9_TH8 LC and transiently transfected into 293F cells as described above. Fabs were purified from culture supernatants using CaptureSelect IgG-CH1 affinity matrix (Life Technologies).

B cell ELISpot assay

To detect IgG-producing cells in blood, BM, spleen, LN, and gut, 96-well Multiscreen-IP filter ELISpot plates (Millipore) were activated using 70% ethanol and washed twice with sterile PBS. The plates were coated with 10 µg/ml anti-human Fcγ/Fcα Ab (Jackson ImmunoResearch) overnight at 4°C. The plates were washed with sterile PBS containing 0.05% Tween-20, and the frozen cells were thawed, plated in complete medium in dilution series, and placed in a 37°C, 5% CO_2 humidified incubator overnight. To detect IgG-producing cells after stimulation, the cells were cultured for 72 h in complete medium supplemented with 5 µg/ml CpG B oligodeoxynucleotides (InvivoGen), 10 µg/ml pokeweed mitogen (Sigma-Aldrich), and 1:1,000 *Staphylococcus aureus* Cowan (Sigma-Aldrich) before plating. The next day, the plates were washed and incubated for 1.5 h with the biotinylated probes: goat anti-human Fcγ (0.025 µg/ml; Jackson ImmunoResearch), 16055 Env trimers (3 µg/ml), or ovalbumin (3 µg/ml) in the respective wells to detect total and antigen-specific Abs. Streptavidin-alkaline phosphatase (Mabtech AB) was added at 1:1,000 dilution in PBS and incubated for 45 min. The plates were washed to develop and visualize spots by the addition of nitro-blue tetrazolium and 5-bromo-4-chloro-3′-indolyphosphate substrate (Mabtech AB) for 5 min in the dark. The reaction was terminated by washing the plates with water. The plates were dried for counting the spots using an Immunospot analyzer (Cellular Technology), and the number of Ab secreting cells per 10^6 cells was calculated as previously described (Martinez et al., 2015; Sundling et al., 2010).

Rep-seq library production and sequencing

We processed all samples as single mononuclear cell suspensions and stored these at −80°C for subsequent analysis. Total RNA extraction from samples from different immune compartments (blood, BM, LN, spleen, and ileum) was performed using the RNeasy kit (Qiagen). First-strand cDNA synthesis was performed at 50°C for 45 min using 0.5 µg of total RNA, isotype-specific primers containing a 21-bp unique molecular identifier and a sequence identical to the Read 2 sequencing primer (Table S1), and Superscript III reverse transcription (Thermo Fisher Scientific). The resulting cDNA was purified using MinElute reaction cleanup kit (Qiagen). Next, 5 µl of cDNA was amplified using the 5′ multiplex primer mix (each of the forward primers targeted the leader sequence of one or more V genes, and each primer contained a tail identical to the Read 1 sequencing primer) and 3′ SR_Universal primer (Table S1). The resultant bands of ∼550 bp were gel purified using the Qiagen gel purification kit, for subsequent Rep-seq library production. 2–10 ng of each gel-purified IgM or IgG product was used in an 8–10-cycle PCR step to introduce Illumina adapters as well as sample-multiplexing indexes. Products from all samples were purified using Ampure XP beads according to the TrueSeq protocol, and the resulting libraries were validated and quantified. The various individually indexed libraries were sequenced on the Illumina MiSeq using the Illumina Version 3, (2 × 300 bp) sequencing kit. 15% PhiX174 DNA was included as a control and as a means of generating diversity within the MiSeq flow cell.

Analysis of sequencing data

The computational analysis of the libraries, including preprocessing, VDJ annotation, and generation of an individualized germline V gene database, was performed with IgDiscover software (http://docs.igdiscover.se; Corcoran et al., 2016). To trace the B cell lineages in multiple immune compartments, two new IgDiscover modules were developed. The Clonotypes module computes the set of clonotypes (lineages) that occur in a dataset. It is after the preprocessing steps of the IgDiscover pipeline, which include paired-end read merging, removal of duplicate sequences, barcode removal, and gene assignment (see IgDiscover documentation). The result is a table in which each row represents a unique merged read pair. Annotations include, among others, the V, (D), and J gene assignments and the CDR3 sequence. The Clonotypes module partitions the sequences into sets of sequences estimated to belong to the same clonotype. Two sequences are considered to belong to the same clonotype if they have (1) identical V and J gene assignments, (2) identical HCDR3 lengths, and (3) similar HCDR3 regions at either the nucleotide or amino acid level, by either percentage identity or absolute number of mismatches, but with at least the first or last *n* nucleotide/amino acid of the HCDR3s being exactly identical. This restriction on the CDR3 "junctions" reduces inclusion of unrelated contaminating lineages. The sequence similarity criterion is applied transitively; that is, two sequences that would otherwise be in different groups are considered to be of the same clonotype if there is a third sequence that is similar enough to both of them. For each group found by clustering the sequences in this way, a representative is chosen. The second module, Clonoquery, works with two input tables of the same type as above. The reference table contains annotations for the sequences in the dataset of interest, and the smaller query table contains sequences whose clonotypes are to be found in the reference table. Queries are looked up individually using the same criterion as described above. Unlike the first module, similarity among reference sequences is ignored; that is, only reference rows directly found to be of the same clonotype are returned.

Phylogenetic analysis

Ab lineage sequences were first deduplicated, storing their frequencies, using preprocessing scripts implemented in the Julia language for scientific computing. To infer the position of the unmutated common ancestor sequence, the V and J were concatenated, with the junction and D gene masked with ambiguous (N) nucleotide, which are treated as missing data during phylogenetic inference. A maximum-likelihood phylogenetic tree

was inferred with FastTree2 (Price et al., 2010) and visualized with FigTree (http://tree.bio.ed.ac.uk/software/figtree/).

GM9_TH8seq732127 Fab production, crystallization, and structure determination

The GM9_TH8seq732127 IgG protein was expressed in HEK293F cells after transfection of HC and LC plasmids. The protein was purified from the supernatant using protein A resin. The purified IgG was cleaved with LysC, and the GM9_TH8seq732127 Fab was further purified by size-exclusion chromatography HiLoad 16/600 Superdex 200 (GE) column using buffer containing 5 mM Hepes, pH 7.5, and 150 mM NaCl. The purified GM9_TH8seq732127 Fab was screened for crystallization using an NT8 (Formulatrix)-dispensing robot. Screening was done with Wizard Precipitant Synergy block no. 2 (Rigaku), Proplex screen HT (Molecular Dimensions), and Crystal Screen HT (Hampton Research) using the sitting drop vapor diffusion method in 96-well crystallization plates (MRC plates, Hampton Research). The protein drop was mixed with reservoir solution in a 1:1 ratio, equilibrated against 40 µl of reservoir solution, and incubated at 20°C. High-quality morphology crystals of the GM9_TH8seq732127 Fab were obtained in screening condition of Crystal Screen HT (Hampton Research) with 4.0 M sodium formate. The screening condition was expanded using the hanging drop vapor diffusion method to obtain diffractable quality crystals. The crystals were cryoprotected in 15% ethylene glycol and 4 M sodium formate. The cryoprotected crystals were flash-cooled in liquid nitrogen, and data collection was done at ALS 5.0.2. The crystals diffracted to 2.26-Å resolution. The collected data were processed using HKL2000 (Otwinowski and Minor, 1997) and imported using Aimless in CCP4 (Collaborative Computational Project, Number 4, 1994). The structures were solved by molecular replacement using Phaser in CCP4 and unpublished solved Fab structure as a search model. The structure building and refinement were performed in Phenix (Adams et al., 2010) and COOT (Emsley and Cowtan, 2004). The refinement statistics are summarized in Fig. S5 B.

Data availability

Rep-seq data from this study were deposited in the European Nucleotide Archive under accession number PRJEB29348. Accession numbers for the individual Rep-seq library are given in Fig. S2. V and J alleles identified in animal D20 by IgDiscover are from GenBank, available under the accession numbers MK111753–MK111853 (V alleles) and MK111854–MK111861 (J alleles). The Env-specific single-cell HC and LC sequences are available from GenBank under accession numbers MK104588–MK105259 and MK105260–MK105280, respectively. Structure factors and coordinates have been deposited in the Protein Data Bank under PDB ID 6U9U. The authors declare that all data supporting the findings of this study are available within the article and its supplemental files or can be obtained from the corresponding author upon request.

Software availability

The Clonotypes and Clonoquery modules are the part of the IgDiscover software, which is available as open source software under the Massachusetts Institute of Technology license from http://docs.igdiscover.se.

Online supplemental material

Fig. S1 shows Env-specific memory B cell sorting FACS gating and epitope-specificity of the isolated mAbs. Fig. S2 shows Ab repertoire sequencing metadata. Fig. S3 shows B cell ELISpot analysis of the different immune compartments 2 wk after the sixth immunization and intraclonal SHM analysis of Ab lineages traced in the BM compartment. Fig. S4 shows alignments of variants displaying increasing SHM for a subset of Ab lineages found in blood. Fig. S5 shows autologous tier 2 neutralizing Ab titers and data collection and refinement statistics for the structural analysis of GM9_TH8seq732127. Table S1 lists primers used for Next Generation Sequencing library production.

Acknowledgments

We thank Dr. Mats Spångberg and Dr. Bengt Eriksson and all personnel at the Astrid Fagraeus Laboratory for expert assistance with rhesus macaques and Novavax, AB, Uppsala, Sweden, for generously making the Matrix-M adjuvant available to this study. We also thank Fondation Dormeur, Vaduz, and the J.B. Pendleton Charitable Trust for generous support of equipment.

X-ray diffraction data were collected at the Berkeley Center for Structural Biology beamline 5.0.2, which is supported in part by the National Institute of General Medical Sciences. The Advanced Light Source is supported by the Director, Office of Science, Office of Basic Energy Sciences, of the US Department of Energy under contract number DE-AC02-05CH11231. This work was funded by an National Institutes of Health P01 HIV Research and Design grant (AI104722) to G.B. Karlsson Hedestam, R.T. Wyatt, M. Pancera, and L. Shapiro; a Swedish Research Council Distinguished Professor grant (2017-00968) to G.B. Karlsson Hedestam; the intramural research program of the Vaccine Research Center, National Institute of Allergy and Infectious Diseases, National Institutes of Health; and a grant from Karolinska Institutet for doctoral education to G.E. Phad.

The authors declare no competing financial interests.

Author contributions: G.E. Phad, P. Pushparaj, R.T. Wyatt, and G.B. Karlsson Hedestam conceived the study. K. Tran and V. Dubrovskaya produced the 16055 NFL TD CC trimers and analyzed mAbs and Fabs. G.E. Phad, P. Pushparaj, M. Àdori, N. Vázquez Bernat, P. Martinez-Murillo, C. Sundling, C. Sorini, V. Dubrovskaya, and E.J. Villablanca processed samples. G.E. Phad, P. Pushparaj, M. Àdori, V. Dubrovskaya, and K. Bhullar isolated and analyzed mAbs. S. O'Dell and J.R. Mascola evaluated Ab neutralizing activity. P. Pushparaj, P. Martinez-Murillo, and M. Àdori performed ELISpot analysis. G.E. Phad, S. Narang, and M. Corcoran performed Rep-seq and analyzed the data. B. Murrell performed phylogenetic analysis. S. Singh, M. Pancera, G. Dionne, and L. Shapiro performed structural analysis. M. Martin wrote software. All authors contributed to the interpretation of data. G.E. Phad and G.B. Karlsson Hedestam wrote the paper with input from the co-authors.

Submitted: 25 June 2019
Revised: 12 September 2019
Accepted: 3 October 2019

References

Adams, P.D., P.V. Afonine, G. Bunkóczi, V.B. Chen, I.W. Davis, N. Echols, J.J. Headd, L.W. Hung, G.J. Kapral, R.W. Grosse-Kunstleve, et al. 2010. PHENIX: a comprehensive Python-based system for macromolecular structure solution. *Acta Crystallogr. D Biol. Crystallogr.* 66:213–221. https://doi.org/10.1107/S0907444909052925

Bonsignori, M., T. Zhou, Z. Sheng, L. Chen, F. Gao, M.G. Joyce, G. Ozorowski, G.Y. Chuang, C.A. Schramm, K. Wiehe, et al. NISC Comparative Sequencing Program. 2016. Maturation Pathway from Germline to Broad HIV-1 Neutralizer of a CD4-Mimic Antibody. *Cell.* 165:449–463. https://doi.org/10.1016/j.cell.2016.02.022

Cirelli, K.M., D.G. Carnathan, B. Nogal, J.T. Martin, O.L. Rodriguez, A.A. Upadhyay, C.A. Enemuo, E.H. Gebru, Y. Choe, F. Viviano, et al. 2019. Slow Delivery Immunization Enhances HIV Neutralizing Antibody and Germinal Center Responses via Modulation of Immunodominance. *Cell.* 177:1153–1171.e28. https://doi.org/10.1016/j.cell.2019.04.012

Collaborative Computational Project, Number 4. 1994. The CCP4 suite: programs for protein crystallography. *Acta Crystallogr. D Biol. Crystallogr.* 50:760–763. https://doi.org/10.1107/S0907444994003112

Corcoran, M.M., G.E. Phad, N. Vázquez Bernat, C. Stahl-Hennig, N. Sumida, M.A. Persson, M. Martin, and G.B. Karlsson Hedestam. 2016. Production of individualized V gene databases reveals high levels of immunoglobulin genetic diversity. *Nat. Commun.* 7:13642. https://doi.org/10.1038/ncomms13642

Davydov, A.N., A.S. Obraztsova, M.Y. Lebedin, M.A. Turchaninova, D.B. Staroverov, E.M. Merzlyak, G.V. Sharonov, O. Kladova, M. Shugay, O.V. Britanova, and D.M. Chudakov. 2018. Comparative Analysis of B-Cell Receptor Repertoires Induced by Live Yellow Fever Vaccine in Young and Middle-Age Donors. *Front. Immunol.* 9:2309. https://doi.org/10.3389/fimmu.2018.02309

Doria-Rose, N.A., C.A. Schramm, J. Gorman, P.L. Moore, J.N. Bhiman, B.J. DeKosky, M.J. Ernandes, I.S. Georgiev, H.J. Kim, M. Pancera, et al. NISC Comparative Sequencing Program. 2014. Developmental pathway for potent V1V2-directed HIV-neutralizing antibodies. *Nature.* 509:55–62. https://doi.org/10.1038/nature13036

Dubrovskaya, V., J. Guenaga, N. de Val, R. Wilson, Y. Feng, A. Movsesyan, G.B. Karlsson Hedestam, A.B. Ward, and R.T. Wyatt. 2017. Targeted N-glycan deletion at the receptor-binding site retains HIV Env NFL trimer integrity and accelerates the elicited antibody response. *PLoS Pathog.* 13:e1006614. https://doi.org/10.1371/journal.ppat.1006614

Emsley, P., and K. Cowtan. 2004. Coot: model-building tools for molecular graphics. *Acta Crystallogr. D Biol. Crystallogr.* 60:2126–2132. https://doi.org/10.1107/S0907444904019158

Francica, J.R., Z. Sheng, Z. Zhang, Y. Nishimura, M. Shingai, A. Ramesh, B.F. Keele, S.D. Schmidt, B.J. Flynn, S. Darko, et al. NISC Comparative Sequencing Program. 2015. Analysis of immunoglobulin transcripts and hypermutation following SHIV(AD8) infection and protein-plus-adjuvant immunization. *Nat. Commun.* 6:6565. https://doi.org/10.1038/ncomms7565

Galson, J.D., A.J. Pollard, J. Trück, and D.F. Kelly. 2014. Studying the antibody repertoire after vaccination: practical applications. *Trends Immunol.* 35:319–331. https://doi.org/10.1016/j.it.2014.04.005

Georgiou, G., G.C. Ippolito, J. Beausang, C.E. Busse, H. Wardemann, and S.R. Quake. 2014. The promise and challenge of high-throughput sequencing of the antibody repertoire. *Nat. Biotechnol.* 32:158–168. https://doi.org/10.1038/nbt.2782

Guenaga, J., V. Dubrovskaya, N. de Val, S.K. Sharma, B. Carrette, A.B. Ward, and R.T. Wyatt. 2015. Structure-Guided Redesign Increases the Propensity of HIV Env To Generate Highly Stable Soluble Trimers. *J. Virol.* 90:2806–2817. https://doi.org/10.1128/JVI.02652-15

Guenaga, J., F. Garces, N. de Val, R.L. Stanfield, V. Dubrovskaya, B. Higgins, B. Carrette, A.B. Ward, I.A. Wilson, and R.T. Wyatt. 2017. Glycine Substitution at Helix-to-Coil Transitions Facilitates the Structural Determination of a Stabilized Subtype C HIV Envelope Glycoprotein. *Immunity.* 46:792–803.e3. https://doi.org/10.1016/j.immuni.2017.04.014

Huang, J., B.H. Kang, M. Pancera, J.H. Lee, T. Tong, Y. Feng, H. Imamichi, I.S. Georgiev, G.Y. Chuang, A. Druz, et al. 2014. Broad and potent HIV-1 neutralization by a human antibody that binds the gp41-gp120 interface. *Nature.* 515:138–142. https://doi.org/10.1038/nature13601

Huang, J., G. Ofek, L. Laub, M.K. Louder, N.A. Doria-Rose, N.S. Longo, H. Imamichi, R.T. Bailer, B. Chakrabarti, S.K. Sharma, et al. 2012. Broad and potent neutralization of HIV-1 by a gp41-specific human antibody. *Nature.* 491:406–412. https://doi.org/10.1038/nature11544

Jiang, N., J. He, J.A. Weinstein, L. Penland, S. Sasaki, X.S. He, C.L. Dekker, N.Y. Zheng, M. Huang, M. Sullivan, et al. 2013. Lineage structure of the human antibody repertoire in response to influenza vaccination. *Sci. Transl. Med.* 5:171ra19. https://doi.org/10.1126/scitranslmed.3004794

Julien, J.P., A. Cupo, D. Sok, R.L. Stanfield, D. Lyumkis, M.C. Deller, P.J. Klasse, D.R. Burton, R.W. Sanders, J.P. Moore, et al. 2013. Crystal structure of a soluble cleaved HIV-1 envelope trimer. *Science.* 342:1477–1483. https://doi.org/10.1126/science.1245625

Klein, F., R. Diskin, J.F. Scheid, C. Gaebler, H. Mouquet, I.S. Georgiev, M. Pancera, T. Zhou, R.B. Incesu, B.Z. Fu, et al. 2013. Somatic mutations of the immunoglobulin framework are generally required for broad and potent HIV-1 neutralization. *Cell.* 153:126–138. https://doi.org/10.1016/j.cell.2013.03.018

Kong, R., K. Xu, T. Zhou, P. Acharya, T. Lemmin, K. Liu, G. Ozorowski, C. Soto, J.D. Taft, R.T. Bailer, et al. 2016. Fusion peptide of HIV-1 as a site of vulnerability to neutralizing antibody. *Science.* 352:828–833. https://doi.org/10.1126/science.aae0474

Kong, R., H. Duan, Z. Sheng, K. Xu, P. Acharya, X. Chen, C. Cheng, A.S. Dingens, J. Gorman, M. Sastry, et al. NISC Comparative Sequencing Program. 2019. Antibody Lineages with Vaccine-Induced Antigen-Binding Hotspots Develop Broad HIV Neutralization. *Cell.* 178:567–584.e19. https://doi.org/10.1016/j.cell.2019.06.030

Kwong, P.D., M.L. Doyle, D.J. Casper, C. Cicala, S.A. Leavitt, S. Majeed, T.D. Steenbeke, M. Venturi, I. Chaiken, M. Fung, et al. 2002. HIV-1 evades antibody-mediated neutralization through conformational masking of receptor-binding sites. *Nature.* 420:678–682. https://doi.org/10.1038/nature01188

Kwong, P.D., J.R. Mascola, and G.J. Nabel. 2013. Broadly neutralizing antibodies and the search for an HIV-1 vaccine: the end of the beginning. *Nat. Rev. Immunol.* 13:693–701. https://doi.org/10.1038/nri3516

Li, M., F. Gao, J.R. Mascola, L. Stamatatos, V.R. Polonis, M. Koutsoukos, G. Voss, P. Goepfert, P. Gilbert, K.M. Greene, et al. 2005. Human immunodeficiency virus type 1 env clones from acute and early subtype B infections for standardized assessments of vaccine-elicited neutralizing antibodies. *J. Virol.* 79:10108–10125. https://doi.org/10.1128/JVI.79.16.10108-10125.2005

Luo, K., H.X. Liao, R. Zhang, D. Easterhoff, K. Wiehe, T.C. Gurley, L.C. Armand, A.A. Allen, T.A. Von Holle, D.J. Marshall, et al. 2016. Tissue memory B cell repertoire analysis after ALVAC/AIDSVAX B/E gp120 immunization of rhesus macaques. *JCI Insight.* 1:e88522. https://doi.org/10.1172/jci.insight.88522

Martinez, P., C. Sundling, S. O'Dell, J.R. Mascola, R.T. Wyatt, and G.B. Karlsson Hedestam. 2015. Primate immune responses to HIV-1 Env formulated in the saponin-based adjuvant AbISCO-100 in the presence or absence of TLR9 co-stimulation. *Sci. Rep.* 5:8925. https://doi.org/10.1038/srep08925

Martinez-Murillo, P., K. Tran, J. Guenaga, G. Lindgren, M. Àdori, Y. Feng, G.E. Phad, N. Vázquez Bernat, S. Bale, J. Ingale, et al. 2017. Particulate Array of Well-Ordered HIV Clade C Env Trimers Elicits Neutralizing Antibodies that Display a Unique V2 Cap Approach. *Immunity.* 46:804–817.e7. https://doi.org/10.1016/j.immuni.2017.04.021

Meng, W., B. Zhang, G.W. Schwartz, A.M. Rosenfeld, D. Ren, J.J.C. Thome, D.J. Carpenter, N. Matsuoka, H. Lerner, A.L. Friedman, et al. 2017. An atlas of B-cell clonal distribution in the human body. *Nat. Biotechnol.* 35:879–884. https://doi.org/10.1038/nbt.3942

Navis, M., K. Tran, S. Bale, G.E. Phad, J. Guenaga, R. Wilson, M. Soldemo, K. McKee, C. Sundling, J. Mascola, et al. 2014. HIV-1 receptor binding site-directed antibodies using a VH1-2 gene segment orthologue are activated by Env trimer immunization. *PLoS Pathog.* 10:e1004337. https://doi.org/10.1371/journal.ppat.1004337

Otwinowski, Z., and W. Minor. 1997. Processing of X-ray Diffraction Data Collected in Oscillation Mode. *Methods Enzymol.* 276A:307–326. https://doi.org/10.1016/S0076-6879(97)76066-X

Parigi, S.M., P. Czarnewski, S. Das, C. Steeg, L. Brockmann, S. Fernandez-Gaitero, V. Yman, M. Forkel, C. Höög, J. Mjösberg, et al. 2018. Flt3 ligand expands bona fide innate lymphoid cell precursors in vivo. *Sci. Rep.* 8:154. https://doi.org/10.1038/s41598-017-18283-0

Pauthner, M., C. Havenar-Daughton, D. Sok, J.P. Nkolola, R. Bastidas, A.V. Boopathy, D.G. Carnathan, A. Chandrashekar, K.M. Cirelli, C.A. Cottrell, et al. 2017. Elicitation of Robust Tier 2 Neutralizing Antibody Responses in Nonhuman Primates by HIV Envelope Trimer Immunization Using Optimized Approaches. *Immunity.* 46:1073–1088.e6. https://doi.org/10.1016/j.immuni.2017.05.007

Pauthner, M.G., J.P. Nkolola, C. Havenar-Daughton, B. Murrell, S.M. Reiss, R. Bastidas, J. Prévost, R. Nedellec, B. von Bredow, P. Abbink, et al. 2019. Vaccine-Induced Protection from Homologous Tier 2 SHIV Challenge in Nonhuman Primates Depends on Serum-Neutralizing Antibody Titers. *Immunity.* 50:241–252.e6. https://doi.org/10.1016/j.immuni.2018.11.011

Phad, G.E., N. Vázquez Bernat, Y. Feng, J. Ingale, P.A. Martinez Murillo, S. O'Dell, Y. Li, J.R. Mascola, C. Sundling, R.T. Wyatt, and G.B. Karlsson Hedestam. 2015. Diverse antibody genetic and recognition properties revealed following HIV-1 envelope glycoprotein immunization. *J. Immunol.* 194:5903–5914. https://doi.org/10.4049/jimmunol.1500122

Price, M.N., P.S. Dehal, and A.P. Arkin. 2010. FastTree 2--approximately maximum-likelihood trees for large alignments. *PLoS One.* 5:e9490. https://doi.org/10.1371/journal.pone.0009490

Ramesh, A., S. Darko, A. Hua, G. Overman, A. Ransier, J.R. Francica, A. Trama, G.D. Tomaras, B.F. Haynes, D.C. Douek, and T.B. Kepler. 2017. Structure and Diversity of the Rhesus Macaque Immunoglobulin Loci through Multiple *De Novo* Genome Assemblies. *Front. Immunol.* 8:1407. https://doi.org/10.3389/fimmu.2017.01407

Sanders, R.W., M.J. van Gils, R. Derking, D. Sok, T.J. Ketas, J.A. Burger, G. Ozorowski, A. Cupo, C. Simonich, L. Goo, et al. 2015. HIV-1 VACCINES. HIV-1 neutralizing antibodies induced by native-like envelope trimers. *Science.* 349:aac4223. https://doi.org/10.1126/science.aac4223

Scheid, J.F., H. Mouquet, B. Ueberheide, R. Diskin, F. Klein, T.Y. Oliveira, J. Pietzsch, D. Fenyo, A. Abadir, K. Velinzon, et al. 2011. Sequence and structural convergence of broad and potent HIV antibodies that mimic CD4 binding. *Science.* 333:1633–1637. https://doi.org/10.1126/science.1207227

Sharma, S.K., N. de Val, S. Bale, J. Guenaga, K. Tran, Y. Feng, V. Dubrovskaya, A.B. Ward, and R.T. Wyatt. 2015. Cleavage-independent HIV-1 Env trimers engineered as soluble native spike mimetics for vaccine design. *Cell Reports.* 11:539–550. https://doi.org/10.1016/j.celrep.2015.03.047

Shen, S., C.W. Pyo, Q. Vu, R. Wang, and D.E. Geraghty. 2013. The essential detail: the genetics and genomics of the primate immune response. *ILAR J.* 54:181–195. https://doi.org/10.1093/ilar/ilt043

Sundling, C., M.N. Forsell, S. O'Dell, Y. Feng, B. Chakrabarti, S.S. Rao, K. Loré, J.R. Mascola, R.T. Wyatt, I. Douagi, and G.B. Karlsson Hedestam. 2010. Soluble HIV-1 Env trimers in adjuvant elicit potent and diverse functional B cell responses in primates. *J. Exp. Med.* 207:2003–2017. https://doi.org/10.1084/jem.20100025

Sundling, C., Y. Li, N. Huynh, C. Poulsen, R. Wilson, S. O'Dell, Y. Feng, J.R. Mascola, R.T. Wyatt, and G.B. Karlsson Hedestam. 2012a. High-resolution definition of vaccine-elicited B cell responses against the HIV primary receptor binding site. *Sci. Transl. Med.* 4:142ra96. https://doi.org/10.1126/scitranslmed.3003752

Sundling, C., G. Phad, I. Douagi, M. Navis, and G.B. Karlsson Hedestam. 2012b. Isolation of antibody V(D)J sequences from single cell sorted rhesus macaque B cells. *J. Immunol. Methods.* 386:85–93. https://doi.org/10.1016/j.jim.2012.09.003

Sundling, C., Z. Zhang, G.E. Phad, Z. Sheng, Y. Wang, J.R. Mascola, Y. Li, R.T. Wyatt, L. Shapiro, and G.B. Karlsson Hedestam. 2014. Single-cell and deep sequencing of IgG-switched macaque B cells reveal a diverse Ig repertoire following immunization. *J. Immunol.* 192:3637–3644. https://doi.org/10.4049/jimmunol.1303334

Tiller, T., E. Meffre, S. Yurasov, M. Tsuiji, M.C. Nussenzweig, and H. Wardemann. 2008. Efficient generation of monoclonal antibodies from single human B cells by single cell RT-PCR and expression vector cloning. *J. Immunol. Methods.* 329:112–124. https://doi.org/10.1016/j.jim.2007.09.017

Walker, L.M., M. Huber, K.J. Doores, E. Falkowska, R. Pejchal, J.P. Julien, S.K. Wang, A. Ramos, P.Y. Chan-Hui, M. Moyle, et al. Protocol G Principal Investigators. 2011. Broad neutralization coverage of HIV by multiple highly potent antibodies. *Nature.* 477:466–470. https://doi.org/10.1038/nature10373

Wang, Y., C. Sundling, R. Wilson, S. O'Dell, Y. Chen, K. Dai, G.E. Phad, J. Zhu, Y. Xiao, J.R. Mascola, et al. 2016. High-Resolution Longitudinal Study of HIV-1 Env Vaccine-Elicited B Cell Responses to the Virus Primary Receptor Binding Site Reveals Affinity Maturation and Clonal Persistence. *J. Immunol.* 196:3729–3743. https://doi.org/10.4049/jimmunol.1502543

Wei, X., J.M. Decker, S. Wang, H. Hui, J.C. Kappes, X. Wu, J.F. Salazar-Gonzalez, M.G. Salazar, J.M. Kilby, M.S. Saag, et al. 2003. Antibody neutralization and escape by HIV-1. *Nature.* 422:307–312. https://doi.org/10.1038/nature01470

Wiley, S.R., V.S. Raman, A. Desbien, H.R. Bailor, R. Bhardwaj, A.R. Shakri, S.G. Reed, C.E. Chitnis, and D. Carter. 2011. Targeting TLRs expands the antibody repertoire in response to a malaria vaccine. *Sci. Transl. Med.* 3:93ra69. https://doi.org/10.1126/scitranslmed.3002135

Wu, X., Z.Y. Yang, Y. Li, C.M. Hogerkorp, W.R. Schief, M.S. Seaman, T. Zhou, S.D. Schmidt, L. Wu, L. Xu, et al. 2010. Rational design of envelope identifies broadly neutralizing human monoclonal antibodies to HIV-1. *Science.* 329:856–861. https://doi.org/10.1126/science.1187659

Wu, X., Z. Zhang, C.A. Schramm, M.G. Joyce, Y.D. Kwon, T. Zhou, Z. Sheng, B. Zhang, S. O'Dell, K. McKee, et al. NISC Comparative Sequencing Program. 2015. Maturation and Diversity of the VRC01-Antibody Lineage over 15 Years of Chronic HIV-1 Infection. *Cell.* 161:470–485. https://doi.org/10.1016/j.cell.2015.03.004

Xu, K., P. Acharya, R. Kong, C. Cheng, G.Y. Chuang, K. Liu, M.K. Louder, S. O'Dell, R. Rawi, M. Sastry, et al. 2018. Epitope-based vaccine design yields fusion peptide-directed antibodies that neutralize diverse strains of HIV-1. *Nat. Med.* 24:857–867. https://doi.org/10.1038/s41591-018-0042-6

Yaari, G., and S.H. Kleinstein. 2015. Practical guidelines for B-cell receptor repertoire sequencing analysis. *Genome Med.* 7:121. https://doi.org/10.1186/s13073-015-0243-2

Yacoob, C., M.D. Lange, K. Cohen, K. Lathia, J. Feng, J. Glenn, S. Carbonetti, B. Oliver, V. Vigdorovich, D.N. Sather, and L. Stamatatos. 2018. B cell clonal lineage alterations upon recombinant HIV-1 envelope immunization of rhesus macaques. *PLoS Pathog.* 14:e1007120. https://doi.org/10.1371/journal.ppat.1007120

Yermanos, A.D., A.K. Dounas, T. Stadler, A. Oxenius, and S.T. Reddy. 2018. Tracing Antibody Repertoire Evolution by Systems Phylogeny. *Front. Immunol.* 9:2149. https://doi.org/10.3389/fimmu.2018.02149

JEM

Supplemental material

Phad et al., https://doi.org/10.1084/jem.20191155

A

Animal ID	D20
Immunization	2 weeks post imm 6
Probe	16055 NFLTDCC
Total PBMCs	15000000
% IgG+ B cells of PBMCs	1.85
total IgG+ B cells in PBMCs	277500
% memory B cells of IgG+ B cells	45.23
% memory B cells of PBMCs	0.8426
total, IgG+ memory B cells in PBMCs	126390
% Env+ mem B cells of CD20+IgG+ cells	1.52
% Env+ mem B cells of the total PBMCs	0.0127
Env+ total mem B cells	1905
Sorted cells	1034
Expressed mAbs	21
Env-specific mAbs	17

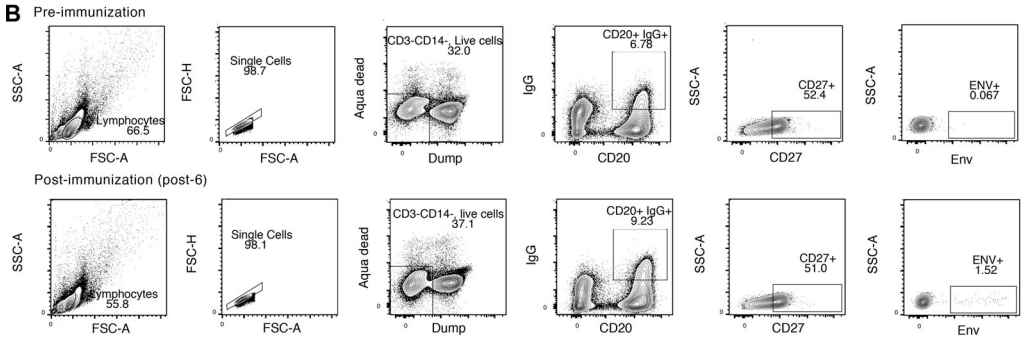

C

Individualized V germline database of animal D20			
Number of IgDiscovered V alleles = 101			
Number of V alleles validated by genomic sequencing = 94 (93%)			
VH family	VH Allele	VH family	VH Allele
1 (n=7)	1K.SEQ_S9938	3 (n=50)	3.63_S7421
	1_2D		3.58_S7764
	1-F*01_S9013		3.44_S7243
	1.59		3.58_S8482
	1.36_S3508_ns		3.30_S9470
	1.16		3.54_S1133
	1_1V		3.9_S4736
2 (n=7)	2.12_S3812		3.44
	2_1P		3.6_S2144
	2.12_S3618		3.9_S6411
	2.25_S1251		3.18_S8778
	2.62_S5657		3_3Z
	2.12		3_4O
	2.25_S2193_ns		3.24_S7175
4 (n=30)	4.34_S7244		3SEQ20_S9125
	4-B*01_S0424		3.10_S8048
	4-C*01_S0972		3_1G_S0150
	4-B*01_S5324		3.18_S2991
	4.22_S3704		3.17_S5625
	4.22_S1537		3.58_S1717
	4.38		3.18_S4823
	4-C*01_S4880		3_2V
	4.11_S0673		3-M*01_S3238
	4.28_S6358		3SEQ17_S2543
	4.37_S2797		3.47_S0569
	4.22_S8697		3_3R
	4.37		3.10_S9408
	4_6F_S5697		3.13_S9311
	4.11_S3326		3_3Q_S0134
	4.11		3.44_S4959_ns
	4.39_S3994		3.2_S9855
	4.34_S8334		3.2_S9938
	4_3Y_S2505		3.42_S2646
	4-9_S2339		3.5_S6633
	4.11_S8588		3.2_S0575
	4.34		3.27_S8819
	4.22_S5131		3.27_S6210
	4.11_S9546		3-F*01_S5150
	4_6B_S8228		3.58_S1171
	4-39_S9152		3.8_S1591
	4.11_S5664		3_3A
	4.38_S9472		3.19_S1419
	4.22_S7765		3.31
	4.38_S7576		3SEQ20_S4842
5 (n=4)	5-B*01_S3407		3.5_S7599
	5.7_S4539		3.8_S7116
	5.7_S5162		3SEQ23_S6450
	5_1H_S8302		3.31_S6406
6 (n=1)	6_B*		3.44_S3154
7 (n=2)	7-B*01_S0001_ns		3_3N_S9643
	7_A*		

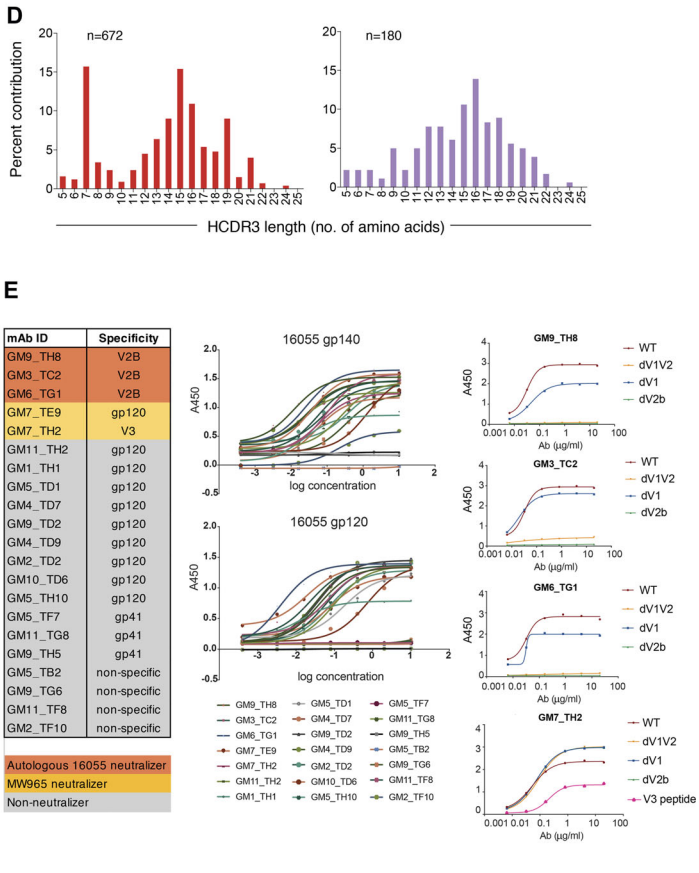

mAb ID	Specificity
GM9_TH8	V2B
GM3_TC2	V2B
GM6_TG1	V2B
GM7_TE9	gp120
GM7_TH2	V3
GM11_TH2	gp120
GM1_TH1	gp120
GM5_TD1	gp120
GM4_TD7	gp120
GM9_TD2	gp120
GM4_TD9	gp120
GM2_TD2	gp120
GM10_TD6	gp120
GM5_TH10	gp120
GM5_TF7	gp41
GM11_TG8	gp41
GM9_TH5	gp41
GM5_TB2	non-specific
GM9_TG6	non-specific
GM11_TF8	non-specific
GM2_TF10	non-specific

Autologous 16055 neutralizer
MW965 neutralizer
Non-neutralizer

Figure S1. **Env-specific memory B cell sorting FACS gating and epitope specificity of the isolated mAbs. (A)** Details from the Env-specific single memory B cell sorting, listing numbers and frequencies of the indicated cell populations. **(B)** Antigen-specific memory B cells were identified as live $CD3^-CD14^-CD20^+$ $IgG^+CD27^+Env^+$ cells as indicated by the FACS gating. The upper panels show preimmunization PBMCs from animal D20 serving as a negative control. The lower panel shows 16055 Env-specific single memory B cells from PBMCs isolated from D20 after the sixth immunization. The numbers indicate population frequencies from the parent gate (one independent experiment). FSC, forward scatter; SSC, side scatter. **(C)** List of IgDiscover-identified VH alleles in D20. **(D)** HCDR3 length distribution shown as the percentage of sequences with a given HCDR3 length of the total number Env-specific single cell sequences (n = 672; upper panel) and the number of clonotypes (n = 180; lower panel). **(E)** List of cloned mAbs with their epitope specificities and neutralizing activities indicated (left). ELISA binding of the mAbs to 16055 Env gp140 or gp120 (middle). ELISA binding of selected mAbs to WT 16055 gp120, gp120ΔV1, gp120ΔV1V2, gp120ΔV2b, and the 16055 V3 peptide (right; representative data from duplicate wells from two independent experiments).

Compartment		Molecule type	Total reads	Merged reads	Barcode clusters	Unique VDJ sequences	Accession numbers
Peripheral blood (PB)	Pre-immunization	IgM	1,173,508	1,146,323	437,620	393,315	ERR2856338
	Post-1	IgG	1,478,331	1,431,796	980,910	902,735	ERR2856339
	Post-2	IgG	1,576,743	1,540,797	510,364	459,191	ERR2856340
	Post-4	IgG	1,040,401	1,035,999	869,121	834,431	ERR2856341
	Post-6	IgG	3,546,531	3,394,147	1,698,475	1,518,699	ERR2856342
Bone marrow (BM)	Pre-immunization	IgG	1,472,783	1,444,670	967,025	896,516	ERR2856343
	Post-2	IgG	1,507,448	1,479,596	987,643	916,660	ERR2856344
	Post-4	IgG	972,964	969,208	763,802	732,740	ERR2856345
	Post-6	IgG	2,075,949	2,069,047	1,502,513	1,436,401	ERR2856346
Inguinal lymph node (iLN)	Post-6	IgG	2,874,018	2,750,523	2,033,643	1,858,215	ERR2856347
Spleen (SL)	Post-6	IgG	2,550,419	2,460,066	1,853,760	1,696,492	ERR2856348
Gut (ileum)	Post-6	IgG	3,777,056	3,673,339	2,086,307	1,915,650	ERR2856349

Figure S2. **Ab repertoire sequencing metadata**. Total reads, number of raw sequences generated using MiSeqs 2X300bp sequencing platform from different tissue compartments and time points from animal D20; merged reads, number of paired sequences; barcode clusters, number of sequences after collapsing sequences with identical barcodes and HCDR3 into a single consensus sequence (including singletons); unique VDJ sequences, total number of uniquely barcoded in-frame Ab sequences (data from one independent experiment).

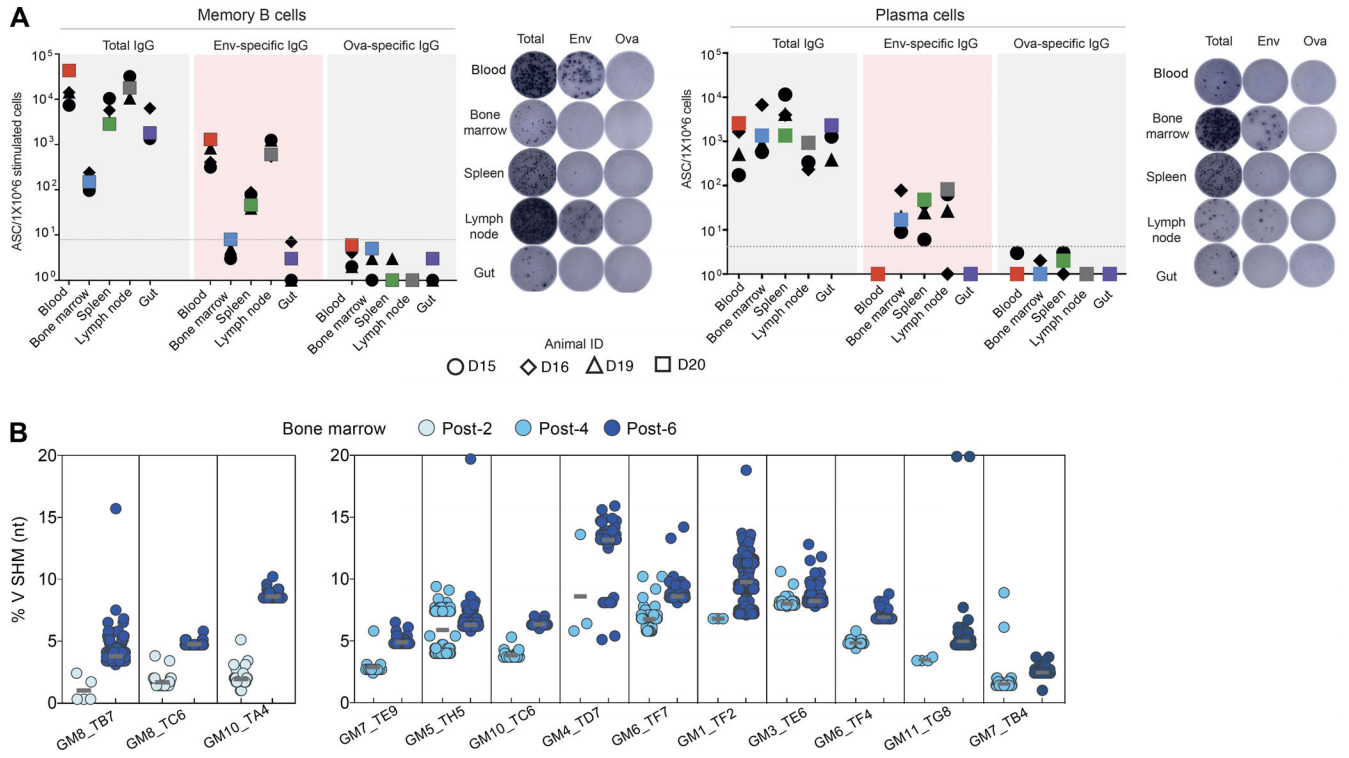

Figure S3. **B cell ELISpot analysis of the different immune compartments 2 wk after the sixth immunization and intraclonal SHM analysis of Ab lineages traced in the BM compartment. (A)** B cell ELISpot assay was performed on PBMC, BM, LN, spleen, and gut samples collected from all four animals, with each symbol in the graph representing one rhesus macaque; D20 is highlighted in color. Total and antigen-specific memory B cells or IgG-secreting plasma cells were enumerated using two different B cell ELISpot formats: with prior in vitro stimulation to differentiate memory B cells into Ab-secreting cells or with direct plating to direct plasma cells present in the sample. Ovalbumin was used as a negative control antigen. The images on the right show representative ELISpot wells from the different samples, where each spot denotes one IgG-secreting cell. **(B)** Level of divergence from assigned germline VH gene sequence at the nucleotide level, shown for individual Env-specific B cell lineages. Each box shows one clonal lineage, with each variant of the lineage identified in the Rep-seq represented as one dot. Data from Rep-seq libraries generated from the BM post-2, post-4, and post-6 time points (representative data from one independent experiment analyzed at least twice).

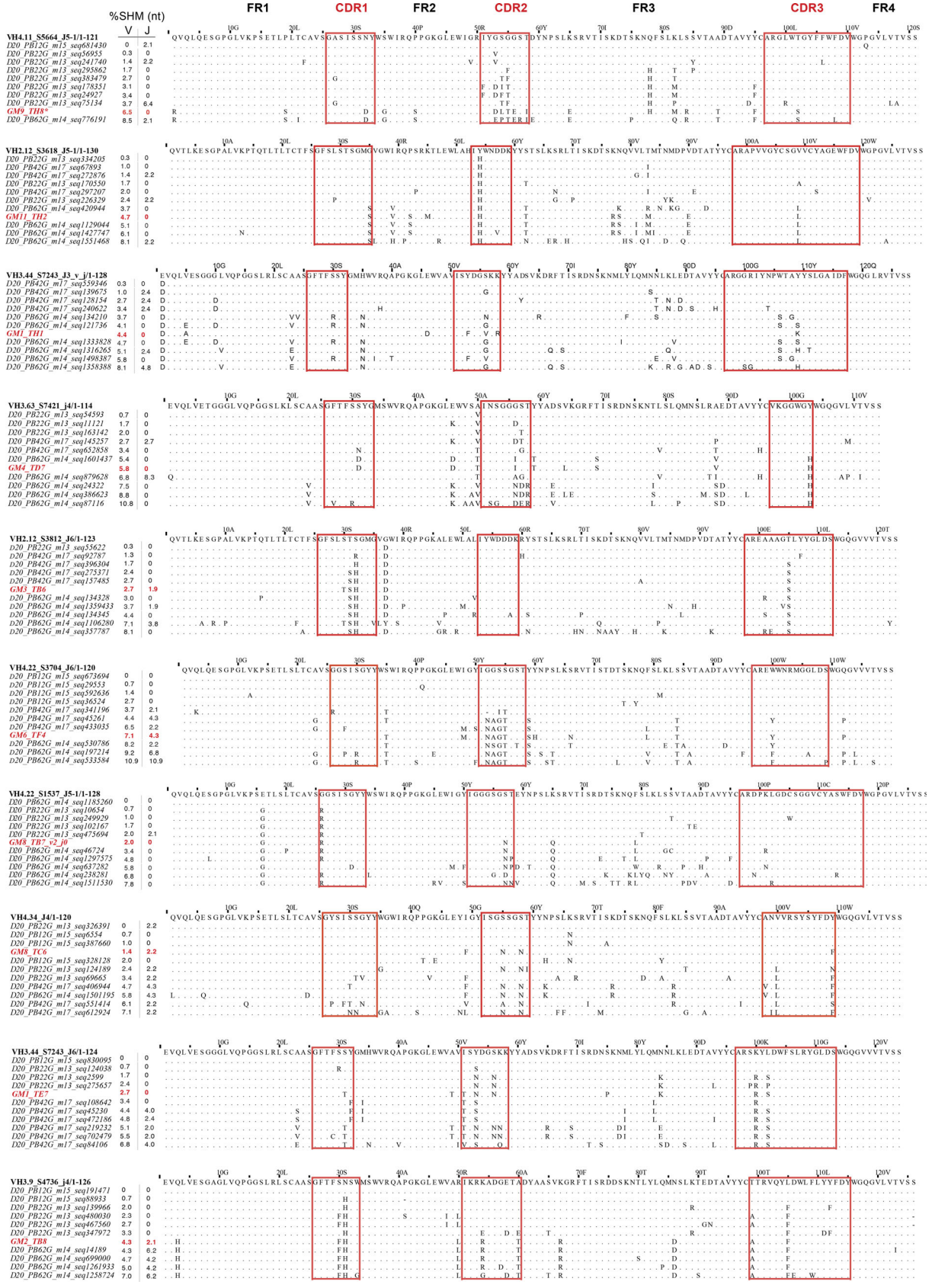

Figure S4. **Alignments of variants displaying increasing SHM for subset of Ab lineages found in blood.** Env-specific Ab HC sequences (red) were aligned to 10 somatic variants, each ranging from low to high SHM. The top row shows the inferred germline sequence of each HC, where the VD and DJ junctions were determined based on the least-mutated variant found in the blood Rep-seq data for each lineage.

A

Name	V SHM (% aa)	Neutralization (IC80, μg/ml)		Neutralization (IC50, nM)		Neutralization (IC80, nM)	
		IgG	Fab	IgG	Fab	IgG	Fab
PB_seq681430_post-1	0	>50	>50	>333	>1000	>333	>1000
PB_seq24927_post-2	7.3	0.068	13.80	0.093	52.80	0.453	276
BM_seq138686_post-2	7.4	0.035	3.06	0.067	12.96	0.233	61.20
iLN_seq1578500_post-6	15.6	0.021	0.675	0.027	2.28	0.140	13.50
SL_seq1387814_post-6	15.6	0.025	0.730	0.033	3.22	0.167	14.60
GM9_TH8_post-6	16.7	0.047	2.01	0.100	8.28	0.313	40.20
BM_seq362970_post-4	16.7	0.054	6.99	0.040	32.00	0.360	140
SL_seq192124_post-6	16.7	0.019	0.542	0.027	2.86	0.127	10.80
SL_seq213526_post-6	18.8	0.010	0.697	0.007	2.64	0.067	13.90
SL_seq597636_post-6	18.8	0.017	0.218	0.033	1.04	0.113	4.36
SL_seq898166_post-6	21.9	0.027	0.131	0.053	0.780	0.180	2.62
iLN_seq732127_post-6	24	0.013	0.083	0.013	0.400	0.087	1.66

B

	GM9_TH8seq732127
Data collection	
Space group	$P4_12_12$
Cell dimensions	
a, *b*, *c* (Å)	147.709, 147.709, 63.200
α, *β*, *γ* (°)	90, 90, 90
Resolution (Å)	50.00-2.26(2.30-2.26)*
R_{sym} or R_{merge}	0.081 (0.865)*
I/s*I*	27.8 (1.6)*
Completeness (%)	100 (100)*
Redundancy	17.9 (15.8)*
$CC_{1/2}$	0.999 (0.837)*
Refinement	
Resolution (Å)	16.78-2.26 (2.30-2.26)*
No. reflections	33193 (1582)*
R_{work}/R_{free}	20.81/24.95 (28.09/32.27)*
No. atoms	6574
Protein	3245
Chain H	3167
Chain L	
Water	126
Ligands	
Sodium	6
Formate ion	10
Ethylene glycol	20
B-factors (Å$_2$)	71.84
Protein	73.88
Chain H	70.16
Chain L	
Water	57.43
Ligands	
Sodium	72.84
Formate	91.81
Ethylene glycol	87.74
R.m.s deviations	
Bond lengths (Å)	0.004
Bond angles (°)	0.649
Ramachadran Favored %	95.75
Ramachadran Outliers %	0.00
MolProbity all-atoms clashscore	4.5
PDB ID	**6U9U**

*Statistics for the highest-resolution shell are shown in parentheses

Figure S5. **Autologous tier 2 neutralizing Ab titers and data collection and refinement statistics for the structural analysis of GM9_TH8seq732127. (A)** Autologous 16055 tier 2 neutralizing activity of the 12 GM9_TH8 variants as IgG or Fabs, shown in the order of increasing SHM (data from one independent experiment). **(B)** Data collection and refinement statistics for the GM9_TH8eq732127 Fab. Statistics for the highest-resolution shell are shown in parentheses (data from one independent experiment).

Table S1 is provided online as a separate Excel file and lists primers used for Next Generation Sequencing library production.